UNIVERSITY OF PAVIA –IUSS SCHOOL FOR ADVANCED STUDIES PAVIA

Department of Brain and Behavioral Sciences (DBBS)

MSc in Psychology, Neuroscience and Human Sciences

Structural connectivity impacts on brain effective connectivity in Developmental Dyslexia as shown by Dynamic Causal Model of visuo-attentive task

Supervisor:

Prof. Claudia Gandini

Co-Supervisors:

Prof. Fulvia Palesi

Prof. Sara Mascheretti

Dr. Gökçe Korkmaz

Thesis written by

Milica Štrbački

Academic year 2023/2024

TABLE OF CONTENTS

LIST OF FIGURES

ABSTRACT

Developmental dyslexia is a neurodevelopmental disorder characterized by difficulties in accurate and fluent word recognition despite normal intelligence and sensory abilities. This thesis explores the brain effective connectivity dynamics by also incorporating the structural information in developmental dyslexia using dynamic causal modeling (DCM) during a visuo-attentive task.

Two groups of participants, typical readers (TR) and those with developmental dyslexia (DD), were assessed using functional magnetic resonance imaging (fMRI) to understand the neural mechanisms underlying altered connectivity patterns identified for the developmental dyslexia. The study involves 40 participants (20 TR, 20 DD) who underwent neuropsychological assessments. MRI data were collected using a 3T scanner, and participants performed Full-Field Sinusoidal Gratings and Coherent Motion Sensitivity tasks to assess visual and attentional processing. The fMRI data were analyzed and conjunction analysis was performed to identify common activation patterns between the tasks. DCM analysis implemented to model the effective connectivity between brain regions, followed by Bayesian model averaging (BMA) to determine the differences in effective connectivity dynamics between two groups in a Fully Connected model and structurally informed model called Cross Brain Model.

The results indicate significant differences in the neuronal effective connectivity patterns between the TR and DD groups. These insights contribute to a deeper understanding of the neurobiological basis of developmental dyslexia and highlight the need for further research to integrate these dimensions comprehensively.

Key words: Developmental Dyslexia, Dynamic Causal Modeling, Effective Connectivity, Bayesian Model Averaging, Functional MRI

1. Developmental Dyslexia

1.1 Definition and history of Developmental Dyslexia

Defining developmental dyslexia can be challenging. Current best definition posits that developmental dyslexia is a neurodevelopmental disorder characterized by slow and inaccurate word recognition (Peterson & Pennington, 2012). It is represented by the discrepancy between inability to acquire visual reading skills, yet possessing intact oral and nonverbal abilities, as well as a genetic background (Stein, 2018). One of the ultimate goals of reading is comprehension, which can be attributed to decoding ability and oral comprehension, with those suffering with developmental dyslexia having difficulties with the former but not the latter (Peterson & Pennington, 2015). The essence of reading is translating letters into sounds they represent (phonemes), which are not consistent and standard acoustic signals. Rather, they depend on the sounds that come before or after it. Firstly, children need to learn that written words consist of separate letters, so that they can translate this into spoken words consisting of phonemes, and unlike speaking this doesn't come automatically, and therefore has to be taught (Stein, 2023). This focus on phonology led to developmental dyslexia being solely associated with an inability to grasp the phonological principle, resulting in the dominance of the 'phonological theory' of developmental dyslexia which posits that developmental dyslexia stems from difficulties in phonological processing, encompassing the ability to recognize and manipulate the sounds of spoken language (Stein, 2023). However, developmental dyslexia isn't the only reason for difficulties with the phonological principle. For instance, teenagers who leave school without proficient reading skills, having comparable skills as an average 11-year-old, are not necessarily dyslexic. Instead, they face a multitude of challenges such as low general ability, inadequate teaching, lack of familial support, truancy, or various socio-economic factors. Moreover, criteria for diagnosing developmental dyslexia, which relied on a gap between reading and oral abilities, have been questioned due to doubts about the reliability of assessing oral comprehension and non-verbal reading skills (Stein, 2023).

Historically, written language is a relatively recent cultural invention, which therefore escaped being subjected to evolutionary pressure (Eden et al., 2016). Brain regions involved in reading subserve other functions such as object recognition, but over the protracted period

of time with formal schooling, they are utilized for reading acquisition which can be difficult for some children (Eden et al., 2016). In particular, Adolf Kussmaul worked with stroke patients who selectively lost their ability to read, while being able to maintain their verbal and non-verbal reasoning skills. Therefore in 1878 he coined the term “word blindness” (Stein, 2018). The term “dyslexia” itself came only a few years later in 1884, derived from Greek ‘dys’ and ‘lexis’ meaning disordered words. The one who coined the term was Rudolph Berlin who worked with stroke patients who lost their ability to spell and read, while maintaining normal speech and oral comprehension. Today we would define this as “acquired dyslexia” (Stein, 2023). Pringle Morgan later described a famous case of ‘Percy’, a boy who was unable to learn to read, even though he had very high verbal and non-verbal intelligence. At the time Morgan named this terminology as “congenital word blindness”, today it can be defined as “developmental dyslexia” (Stein, 2018). Due to Morgan’s interpretation of the disorder being a hereditary defect affecting visual processing of words, while leaving verbal and non-verbal reasoning skills relatively intact, this view has remained until the mid-20th century (Stein, 2018).

1.2 Epidemiology of Developmental Dyslexia

Today dyslexia, encompassing both developmental dyslexia and acquired dyslexia, is the most prevalent learning disability affecting 5-12% of English-speakers, with slightly lower rates for other writing systems, due to mapping of English orthography not being consistent between sound and print (Eden et al., 2016). Dyslexia research has historically for this reason been highly Anglocentric, which posits English-related points (Peterson & Pennington, 2012). Recent cross-cultural research has shown that those struggling with reading of languages with more consistent mapping compared to English, have less severe reading problems. Furthermore, issues that persist over languages which are more useful for the purpose of comparison are reading fluency, speed of reading connected text and spelling (Peterson & Pennington, 2012). Incidence of developmental dyslexia is 2-3 times higher in males than in females and it is considered highly heritable with an estimated 30-50% chance of passing from parent to child (Eden et al., 2016). Specific learning disorders that primarily affect reading ability, can often co-occur with other disorders or conditions. Some of the disorders that are commonly comorbid with developmental dyslexia include ADHD, Language Impairment (LI) and Speech Sound Disorder (SSD) (Peterson & Pennington, 2012). Clinical features of developmental dyslexia depend on the severity of deficits and the

presence of comorbidities (Demonet et al., 2004). Also, comorbidity of reading and math difficulties was found to be approximately 25%, explaining the struggles of children with developmental dyslexia more broadly in school (Peterson & Pennington, 2012).

1.3 Theories of Developmental Dyslexia

Lack of understanding of developmental dyslexia led to numerous new theories emerging to explain its underlying causes. A valuable theory should not only consolidate existing knowledge about the phenomenon but also propose potential causes. Following is an elaboration on some of the most influential theories of developmental dyslexia: the Phonological Theory, the Magnocellular Theory, the Cerebellar Deficit Theory, the Dyslexia Automatization Deficit Hypothesis, the Visual Attention Span Deficit Theory.

Starting with one of the most widely accepted theories explaining developmental dyslexia *"Phonological Theory"* which explains developmental dyslexia as it is primarily characterized by difficulties in phonological processing, which involves the ability to recognize and manipulate the sounds of spoken language. This theory particularly posits that those with developmental dyslexia fail to read because they are unable to learn how to separate the sounds in a word to match with its visual representation. This has been named "phonemic awareness" and can be assessed utilizing pseudo-words. "Phonological awareness" early on can be acquired by practicing rhyme, alliteration, and word games. Linguistic and reading competences are strongly predicted by successful emergence of phonological awareness (Stein, 2018). Primary concern with this theory is that it is hard to distinguish developmental dyslexia from other causes of reading failure just based on phonology. Whether or not there is a discrepancy between oral and reading abilities, phonological problems are the same (Stein, 2019).

Another theory is the *"Magnocellular Theory", which is* based on the importance of the visual magnocellular system for timing visual events in reading (Stein,2001). Magnocellular neurons got their name from their size (magnus=large). The larger the neuron, the faster all the processes involved in the transmission of the signal. Due to their size they aren't sensitive to fine details but are much faster in responding. They aren't involved in color vision, but are involved in timing of light inputs, and therefore are sensitive to movement. Magnocells project their axons to the magnocellular layer of the lateral geniculate nucleus (LGN) in the thalamus, and then further to the primary visual cortex (V1). Besides the magnocells, we can

distinguish parvocells which project to the parvocellular layer of LGN and further to the striate cortex (Stein, 2019). As previously mentioned, these two cell types have different roles in processing visual stimuli. Magnocells are mainly responsible for processing of low spatial frequency, and high temporal frequency, but not color. On the other hand, the parvocells are responsible for high spatial frequency, and low temporal frequency and it also conveys color information. So it can be said that the magnocells are mainly involved in motion, brightness, and depth processing, and parvocells are involved in fine detail and color processing (Atkinson, 1992). In addition, sensitivity to visual motion seems to predict how well orthographic skills will develop in regard to reading. Those with developmental dyslexia are slower at recognizing individual letters and at sequencing them correctly, with magnocellular-dorsal attention stream being responsible for both of these functions (Stein, 2001). The magnocellular-dorsal attention stream is dominated by magnocells and specialized for the deployment of visual attention and visuomotor control. Moreover, the visual motion area V5/MT is mainly supplied by the magnocellular system and is active during visual attention and visually guided movements in normal population, and much reduced in developmental dyslexia (Stein, 2019). The cerebellum, which is affected in developmental dyslexia, is the head ganglion of the magnocellular system which plays a role in binocular fixation and inner speech for sounding out words (Stein, 2001). In dyslexia, the accuracy of their eye fixation seems also to be compromised, as the magnocellular system would usually detect any unwanted eye movements which would cause the text to appear to move around. Even when silent reading, which doesn't require sounding out the words, the shape of the letters still needs to be associated with a particular sound, and the visual attention must be properly cued. The visual/auditory cross modal cueing of attention is affected in developmental dyslexia impacting their ability to perform even silent reading. However, the primary concern with this theory is the possibility that magnocells have reduced sensitivity as a result of failing to learn to read, thereby getting less visual skills practice, and not vice versa (Stein, 2019).

The "*Cerebellar Deficit Theory"* of developmental dyslexia, originally proposed by Nicolson, Fawcett and Dean, posits that cerebellar dysfunction, particularly impaired procedural learning, can provide an explanation for both the reading difficulties and the non-literacy symptoms associated with developmental dyslexia. These non-literacy symptoms encompass issues like poor handwriting, laborious learning, and challenges with visual sequencing (Stoodley & Stein, 2013). The foundation of the "*Cerebellar Deficit*

Theory" is cerebellum which exhibits activity not only during speech but also during silent reading, passive language processing, and visually guided movements such as the eye movements necessary for reading text. Alternatively, certain cerebellar functions, including the direction of attention, error detection, timing and sequencing, as well as implicit and associative learning, may play a role in reading (Stoodley, 2014). As further proof of cerebellar involvement in reading, traumatic brain injury studies have found that cerebellar damage results in reading difficulties in both children and adults (Scott et al., 2001). The cerebellum enables automatic behaviors by constantly adapting to the environment by interacting with the prefrontal cortex in order to be able to anticipate outcomes and adapt accordingly to be able to control motor behavior. The interaction between cerebellum and executive function might explain why developmental dyslexia is less prevalent in countries who use language that has more incongruence between spelling and pronunciation of words (Smith-Spark & Gordon, 2022). Biologically speaking, cerebellar deficit could be either an alternative or happening in parallel to the magnocellular system abnormality (Nicolson et al., 2001).

Another theory proposed by Nicolson and Fawcett (1990) for the cerebellar involvement in developmental dyslexia is the "*Dyslexia Automatization Deficit hypothesis"* which posits that dyslexia-related problems stem from a lack of automaticity and the necessity to allocate attentional resources consciously (Stoodley & Stein, 2013). Especially, adults with developmental dyslexia showed reduced activation of the right cerebellar cortex during the learning of novel motor sequences and the performance of pre-learned sequences, as well as increased frontal activation in developmental dyslexia patients, which was hypothesized to compensate for the reduced activation of the cerebellum (Smith-Spark & Gordon, 2022). Cerebellar impairment is also likely to cause, either directly or indirectly, the "phonological core deficit" (Nicolson et al., 2001), which refers to a specific impairment in the processing or awareness of the sounds of language, particularly in relation to reading and language learning (Stanovich, 1988).

Lastly, the "*Visual Attention Span (VAS) Deficit hypothesis"* stands out by stating that some dyslexic people suffer from poor visual attention capacity, affecting the number of visual elements they can process simultaneously in a multi-element array, resulting in reduced VAS. This hypothesis initially stems from the theoretical framework of the multi-trace memory model. According to this model, VAS deficit results from a reduced distribution of visual attention across the input letter string, therefore affecting letter recognition with no impact on

phonological processing. Moreover, VAS would depend on the activation of the bilateral superior parietal lobules (SPLs), a brain region belonging to the dorsal attentional network but not to the language network (Valdois, 2022).

1.4 Attentional networks and their involvement in Developmental Dyslexia

Research indicates that visual attention deficits significantly contribute to the reading challenges experienced by individuals with dyslexia. Specifically, children with dyslexia exhibit deficiencies in various visual abilities, including visual perception, visual temporal processing, and the swift deployment of attention (Peters et al., 2019). Moreover, during the pre-reading phase, the proficiency of visual attention skills serves as a predictive factor for subsequent reading development (Taran et al., 2022). In their study, Morken et al. (2014) found that children with dyslexia exhibited heightened cortical activation, especially in temporal and frontal areas, suggesting that dyslexic children may use more neural resources compared to their peers, highlighting potential compensatory mechanisms at play.

1.4.1 Attentional networks

Attention is one of the most studied areas in psychology. By definition, attention is a process of selecting an active idea or an environmental feature to focus on, allowing us to prioritize between different options. Moreover, it can be focused on different areas of the visual field and can easily switch between points (i.e. when looking at a book, one can pay attention to the words written allowing them to catch smaller mistakes, or to the page as a whole) (Raz, 2004). Historically, there has been a general assumption that visual attention is a function of right hemisphere only, however multiple neuroimaging studies have to this day shown bilateral fronto-parietal activation, with dominance in the right hemisphere in majority, but not all, of the population (de Shotten et al., 2011).

Visual attention encompasses orienting, vigilance and executive attention. Firstly, when talking about **orienting** of visual attention, we can distinguish between overt, that is directing the eye movement towards the area of interest, and covert, which is assigning priority to an area without consequent eye movement and orienting (Fernandez-Duque & Posner, 2001). Both of these orienting types have been shown to activate brain areas such as precentral gyrus and areas in the parietal lobe including superior parietal, temporoparietal, lateral inferior parietal areas, frontal eye fields, as well as subcortical structures such as superior culliculus and thalamus (Fernandez-Duque & Posner, 2001). It is important to note that there is a prevalent theory, *supramodal orienting system theory*, which states that selecting of the relevant information can be also based on non-spatial features such as color or time (Fernandez-Duque & Posner, 2001). Orienting system is comprised of the dorsal attention

network (DAN) and ventral attention networks (VANs), supporting the ability to prioritize sensory input and to shift attention, elucidating both bottom-up reorienting processes and top-down visuospatial functions, however flexible attentional control can only be implemented by dynamic interactions of both systems. This interaction is overseen by frontal areas such as the inferior and middle frontal gyrus (Vossel et al., 2013). Secondly, **vigilance**, alternatively named alertness or sustained attention, is an ability to achieve and sustain an alert state in preparation for stimulus. We differentiate between phasic vigilance (task specific), and intrinsic vigilance (a general cognitive control of arousal), a foundational form of attention on which other attentional functions rest. Phasic vigilance allows us, for a short period of time after an alerting stimulus, to increase the processing efficiency of features in the environment (Goldfarb & Shaul, 2013). Although the relationship between phasic and intrinsic vigilance (arousal) is poorly understood, there are findings that vigilance in unwarned situations (intrinsic vigilance) heavily relies on a right hemisphere cortical and subcortical network with the anterior cingulate cortex as a central structure attention (Raz & Buhle, 2006). Generally, when a person is in an alert state, regardless of the actual presence of the stimulus, there is an increase in brain activation, especially in the right fronto-parietal areas (Fernandez-Duque & Posner, 2001), or alternatively locus coeruleus (Berger & Posner, 2000). On the other hand, it is important to distinguish the differences between the two attention systems. Primary difference between the alerting and orienting systems is the opposite way they recruit attention. The alerting system is stimuli driven, contrary to the spatial orienting system which is goal driven. The alerting system engages global attention, contrary to the spatial orienting system which is responsible for selectively orienting attention to a certain restricted location. Due to the inability of these two functions to coexist, one might need to switch off one system when operating the other. Neurologically, it has been suggested that the right temporal parietal junction (TPJ) acts as a bridge between these systems. This area receives input from other brain structures regarding novel or alerting stimuli in the environment and in turn inhibits the cycle of the spatial orienting goal directed system (Goldfarb & Shaul, 2013). Lastly, **executive attention** also namely, supervisory, selective, conflict resolution and focused attention (Raz & Buhle, 2006) involves effortful control of attention, and is prevalent in task switching, inhibitory control, conflict resolution, error detection, allocation of attentional resources, planning, and decision making. In particular, the neuronal activation is present in the anterior cingulate and supplementary motor area, the orbitofrontal cortex, the dorsolateral prefrontal cortex, and portions of the

basal ganglia and the thalamus (Fernandez-Duque & Posner, 2001) that are all contribute to the executive functions and attention.

1.4.2 Attention and Developmental Dyslexia

Attention plays a significant role in developmental dyslexia that affects not only reading and learning, but also affects various cognitive processes such as attention (Lewandowska et al., 2014). Therefore addressing attentional difficulties through targeted interventions and strategies can help dyslexic children improve their reading skills, academic performance, and overall quality of life. When considering the reading impairments, it can be suggested that particularly visual attention processing can be affected, which could in part be explained by the faulty simultaneous activation of the angular gyrus together with visual attention-related brain areas (Taran et al., 2021). Further proof is carried from multiple different tasks, on which, in addition to reading difficulties, people with developmental dyslexia have been shown to have difficulties in, specifically based on the executive and orienting attention systems, but not the alerting system (Goldfarb & Shaul, 2013). Dyslexia-related reading difficulties have been shown to possibly stem from impairment in the executive and attentional control functions of the sluggish attentional shifting (SAS), accompanied with deficient results on tasks dealing with performing visuospatial working memory and novel visual patterns. Moreover, failure of the executive control to supervise the functioning of the phonological loop and the visuospatial sketchpad could possibly help give a full explanation of the executive function problems manifested by those with developmental dyslexia (Smith-Spark & Gordon, 2022).

In developmental dyslexia, multiple regions that are a part of visuo-attentional network seem to be functioning inefficiently, causing an abnormal serial selection of graphemes in words leading to difficulties with reading fluently and accurately. Alternatively, compared to patients with developmental dyslexia, typical readers seem to recruit dorsal attentional networks (DAN) along with the angular gyrus more. Issues with integration of visual attention processes and executive functioning in developmental dyslexia can be explained by the ventral attentional network (VAN) being functionally connected to the fronto-parietal network in typical readers, but not in developmental dyslexia patients (Taran et al., 2022).

1.4.3 Cerebellar involvement in Attention

Morphological changes in cerebellum have been associated with attentional deficits in different populations and amongst different pathologies including Autism Spectrum Disorder, Attention Deficit Hyperactivity Disorder and Developmental Dyslexia (Stoodley, 2014). More proof of the link has been shown through studies of cerebellar injury patients (Gottwald et al., 2003). A study done by Mannarelli and colleagues (2019), aside from its involvement in selective attention and attentional shifts, further establishes a role of the cerebellum in the functioning of the attentional networks, particularly the executive network. For instance, during an attention task, cerebellum showed increased connectivity with dorsal visual stream regions including posterior parietal cortex (PPC) and left secondary visual cortex (V5). Additionally, the cerebellum is suggested to maintain internal models related to visual inputs (D'Angelo, 2018). Executive control as well as other higher cognitive functions have been linked to cerebellar regions Crus I and Crus II (Kellermann et al., 2012). Furthermore, recent research by Bukhari et al. (2022) highlights the importance of assessing causal interactions between the cerebellum and cerebral cortex, utilizing Dynamic Causal Modeling (DCM) which allows for the identification of directional influences and dynamic relationships between brain regions, providing a deeper understanding of how cerebro-cerebellar interactions contribute to cognitive functions relevant to dyslexia.

1.5 Genetics of Developmental Dyslexia

Genetics play a significant role in developmental dyslexia, with numerous studies indicating a strong genetic component to the disorder. Although it is highly unlikely that a simple link between developmental dyslexia and genetic data exists, interest in the "genetic dissection" still persists. The notion of heritability remains dynamic, as the extent to which genes contribute to total variance is influenced by factors such as variability in exposure to unidentified environmental risk factors and the specific attributes of the studied population (Williams & O'Donovan, 2006). Such endeavors offer the potential for early identification of individuals at heightened risk and facilitate diagnosis in cases where symptoms present ambiguously. Additionally, ongoing research on genetic involvement can lead to advantages in understanding and interventions from an early age (Fisher & DeFries, 2002).

While the precise genetic factors underlying developmental dyslexia remain uncertain, it is evident that the disorder does not manifest randomly within the population. This assertion is supported by the elevated risk of occurrence observed among individuals with a familial history of the condition (Scerri & Schulte-Korne, 2009). Known potential candidate genes for developmental dyslexia are DYX1C1, KIAA0319, DCDC2 and ROBO1, which could be responsible for cortical malformations involving neuronal migration and axon growth (Scerri et al. 2010). These would result in faulty cortico-cortical and cortico-thalamic circuits, involved in multiple processes (e.g. perceptual, cognitive and sensorimotor) that play a key role in learning
(Galaburda et al., 2006).
Lastly, Deco et al. (2021) studied how regional differences in gene expression across the brain affect dynamic interactions and functional integration within neural networks. Using computational models and empirical data, they found that these gene expression variations significantly influence the specialization and connectivity patterns of neural circuits.

2. MRI Physics Fundamentals

2.1 Discovery and characteristics of Magnetic Resonance Imaging

MRI stands out as an extraordinary imaging technology, providing exceptional soft tissue contrast with high spatial resolution. It presents a tomographic 3D view and the ability to capture dynamic physiologic changes. By adjusting the acquisition parameters of MR images, one can generate images that depict a vast range of physical and physiologic phenomena, drawing on the physics of nuclear magnetic resonance (NMR). Importantly, MRI achieves all of this in a noninvasive manner, allowing for safe repeated scans within well-defined technical constraints, without known harm (Plewes & Kucharczyk, 2012).

Magnetic resonance imaging (MRI) has without a doubt been one of the best inventions of modern medicine. For their contribution to the creation and advancement of this technique four people have been awarded the Nobel Prize. Firstly, Raymond Damadian received his Nobel Prize in 1971 for the discovery of different relaxation times in tumor tissue compared to normal tissue. Following that discovery, Paul Lauterbur discovered that the signal can be assigned a specific spatial position by introducing the magnetic field gradients, eventually receiving his Nobel Prize in 1973. Quickly after in 1974 and 1975, Sir Peter Mansfield and Richard Ernst contributed with their inventions allowing the possibility of selecting a specific plane or a slice of an object and the ability to assign the signal components coming from each spatial position using what is known as the Fourier Transform, respectively (Dreizen, 2004).

2.2 Fundamentals of Magnetic Resonance Imaging

Majority of the imaging we are able to perform today is based on the spin of a singular proton of Hydrogen (^{1}H). As long as they have an odd number of protons, other nuclei are also able to exhibit spin (e.g., Calcium), ^{1}H is just more commonly used, considering the amount of ^{1}H we have in our body and brain due to its natural constitution being mostly water (Plewes & Kucharczyk, 2012).

To be able to exploit the electromagnetic properties of ^{1}H it is necessary to introduce a magnetic field. In MRI, this magnetic field is called B_0. B_0 is constant, it has a direction and magnitude. When a proton is introduced to the B_0 it starts precessing around it at Larmour frequency (ωL), expressed by the following formula (2.1):

$$\omega L = \gamma B0 = \omega 0$$

(2.1)

As briefly mentioned before, spin is the key factor. Spin has the spin quantum number (I) which parametrizes the intrinsic spin of particles. It can only be in multiples of ½. Each nucleus can have only a certain number of spin states (m), depending on I.

$$m = I, (I-1), (I-2), \ldots, -I$$

(2.2)

For ^{1}H, $m = -\frac{1}{2}, +\frac{1}{2}$. Therefore, spin or intrinsic angular momentum (P) can be expressed by:

$$P = h/2\pi\sqrt{I(I+1)}$$

(2.3)

Where h is the Plank constant and I is the spin quantum number.

When we have P, we can associate a dipolar magnetic moment (μ) via gyromagnetic constant (γ) which is a characteristic of each nucleus (Brown et al., 2014). We can express this in a formula:

$$\mu = \gamma P$$

(2.4)

The response of a system to a magnetic field is described by its magnetization, denoted as M. When no external magnetic field ($B_0 = 0$) is present, the spins within the system are randomly oriented, resulting in a net magnetization of 0.

Prior to the introduction of the external magnetic field (B_0), each magnetic dipole (μ) in the system is randomly oriented. However, when the magnetic field (B_0) is applied, these dipoles begin to precess at the Larmour frequency. They align either parallel or antiparallel to the direction of B_0, with a slight preference for alignment parallel to B_0. This alignment adds up, resulting in a net positive magnetization (M). Magnetization (M) can be represented as a vector, comprising both a longitudinal component (M_z) and a transverse component (M_{xy}).

With enough time in the magnetic field, the magnetization M reaches a stable equilibrium value, denoted as M_0 (Huettel et al., 2008).

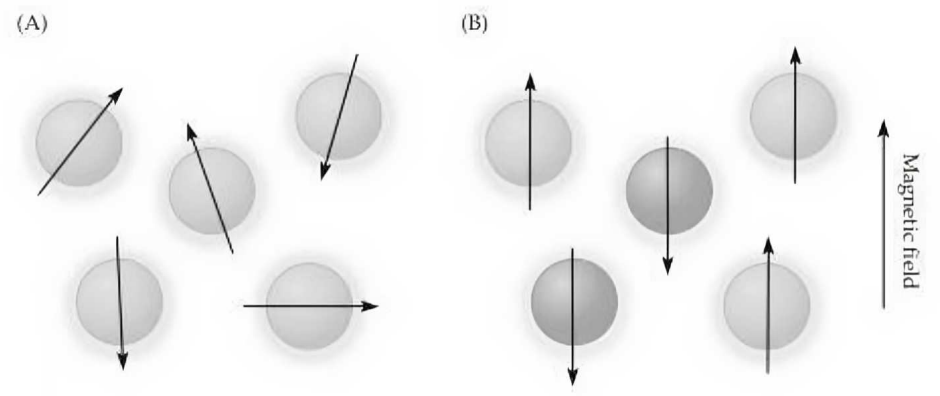

Figure 2.1 Spin axis alignment. (A) Random alignment of spin axis of protons in the absence of an external magnetic field. (B) Introduction of an external magnetic field allows for the spin axis of each proton to be oriented either parallel or antiparallel to the magnetic field (Huettel et al., 2008).

When M_0 aligns with B_0, it becomes challenging to measure. To overcome this, one can aim to reorient M_0 perpendicular to B_0, which is achieved while the system is in equilibrium. The reorientation can be achieved by interacting with M_0 using an electromagnetic field called $B_1(t)$, which is generated by a transmission coil. Moreover, for an effective reorientation, $B_1(t)$ must meet specific criteria with the oscillation at the Larmour frequency, to be positioned orthogonally to B_0, and to have an amplitude (B_1) and duration that allow alignment of $M_1(t)$ with the transverse plane defined by B_0 and $B_1(t)$. In that respect, a radiofrequency (RF) receiver coil can then be used to detect the signal from the magnetization $M_{xy}(t)$, which is precessing in the xy plane around B_0. This detection creates a variable magnetic field flux in the RF receiver coil (Giovannetti et al., 2014).

2.3 Image reconstruction

Recorded is a signal from the brain in "time", which oscillates in the radiofrequency spectrum and encompasses several frequency components. This signal fills k-space. K-space is a mathematical representation of the spatial frequency domain, containing all spatial frequency information of the MRI signal (Plewes & Kucharczyk, 2012). Fourier transform plays a vital role by combining frequency, phase, angle, and amplitude elements to derive stripe patterns crucial for image reconstruction. Each image corresponds to a unique array of these patterns, summarized within k-space data. The center of the k-space, maximum

amplitude of the signal, contains all the information about the image, while the details are in the edges of the k-space. MRI uses magnetic field gradients to distinguish different spatial positions, by making slight variations of the static magnetic field B_0, along specific spatial directions superimposed on B0, generating frequencies of precession dependent on the position. Each signal can be described in time or in frequency, with the possibility to convert these two representations from one to the other using the Fourier transform. Fourier transform is a mathematical operation allowing for the extraction of the signals of various components coming from different spatial positions (Plewes & Kucharczyk, 2012).

Frequency encoding and phase encoding are two fundamental MRI techniques used to spatially encode the received signal. Frequency encoding and the use of frequency encoding magnetic field gradients allows to distinguish positions along one axis. Phase encoding and the use of phase encoding magnetic field gradients allows to distinguish positions along an axis orthogonal to the one used for frequency encoding by controlling the initial value of the signal from the spin, also known as its phase. A third direction, orthogonal to both phase and frequency encoding directions, called Z axis, uses slice selection magnetic field gradients, with which we can image the whole object (Haacke et al., 1999).

2.4 Relaxation

As soon as the radiofrequency (RF) pulse is switched off the protons start to fall out of phase with each other and return to equilibrium, otherwise described as, protons relax. During this relaxation process within the receiver coils, transverse magnetization M_{xy} induces a signal known as Free Induction Decay (FID) (Weishaupt et al., 2006). Return to the equilibrium is based on two mechanisms:

1. Longitudinal spin-lattice relaxation (T1)
2. Transverse spin-spin relaxation (T2)

Longitudinal spin-lattice relaxation (T1) is a phenomenon in which magnetization M_{xy} recovers its alignment along the Z axis, the direction of the static magnetic field B_0, due to the exchange of energy between spins and the lattice. The exchange of energy is dependent on the microstructure as exchange is more efficient when there are more collisions between spins and lattice. T1 is a time constant that is a measure of time needed for the magnetization M(t) to go back to equilibrium, after the system is perturbed with the $B_1(t)$ radiofrequency pulse (Hashemi et al., 2012). Formula 2.5 illustrates how the longitudinal magnetization increases from an initial perturbed state towards its equilibrium value exponentially over time, with the rate of increase determined by the T1 relaxation time constant. As time increases, the exponential term *e* approaches zero, causing the magnetization to approach its equilibrium value M_0.

$$M_z(t) = M_0(1 - e^{-t/T_1}) \tag{2.5}$$

T_1 is the exponential constant corresponding to the point when the magnetization M_z ($t=T_1$), which was zero immediately after the B_1 pulse, has recovered 63% of the equilibrium magnetization M_0.

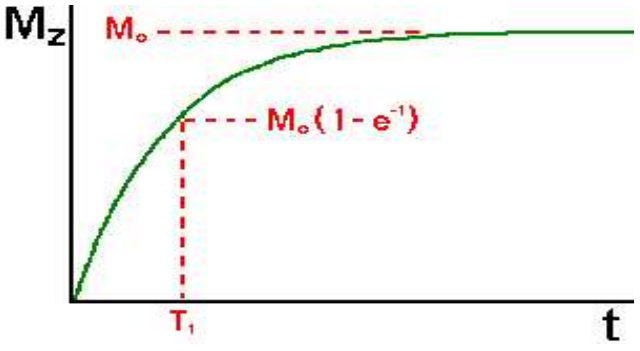

Figure 2.2. Illustration of T1 relaxation constant. M_Z starts from 0 and grows back to M_0 with an exponential curve (Hashemi et al., 2012).

Transverse spin-spin relaxation is a phenomenon in which due to interaction between spins there is a loss of coherence, and therefore energy. This phenomenon can be pictured as dephasing of the spins, consequence of which is the disappearance of the transverse magnetization M_{xy} (Hashemi et al., 2012). Formula 2.6 illustrates how the transverse magnetization exponentially decays over time, with the decay rate determined by the T2 relaxation time constant. As time progresses, the exponential term *e* approaches zero, resulting in the decay of the transverse magnetization towards zero.

$$M_{xy}(t) = M_{xy}(0)\, e^{-t/T_2} \tag{2.6}$$

T2 is an exponential constant corresponding to the time needed for M_{xy} (t=T2) to be reduced by 63% of its initial value.

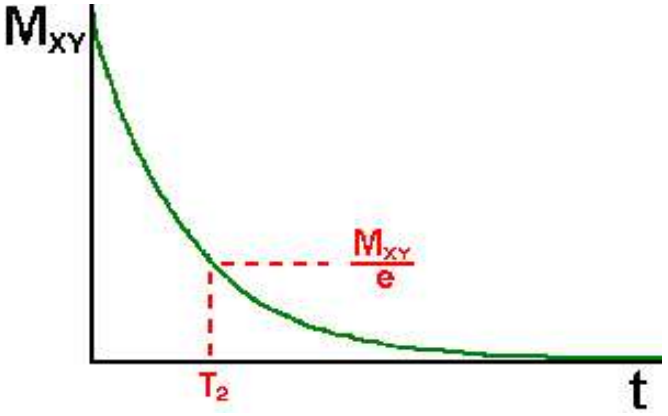

Figure 2.3. Illustration of T2 relaxation constant. The decay is characterized by a time constant, T2, which corresponds to the time needed for M_{xy} to be reduced by 63% of its initial value (Hashemi et al., 2012).

As B_0 is not homogeneous, with local variations in Larmour frequency and consequent phase dispersion between the spins, the disappearance of M_{xy} is affected, FID decays faster than if B_0 was perfectly uniform. Therefore, it's important to introduce transverse relaxation constant T2* which accounts for the faster FID (Hashemi et al., 2012).

2.5 Sequences and different image contrasts

Understanding MRI pulse sequences offers insight into the imaging process. By manipulating various timing parameters, it becomes feasible to generate images that capture distinct contrasts corresponding to different relaxation mechanisms. This capacity to adjust timing parameters enables the creation of images tailored to highlight specific tissue characteristics, facilitating enhanced diagnostic capabilities in MRI imaging (Plewes & Kucharczyk, 2012).

Tissues can be divided into:

- fluids
- water-based tissue
- fat-based tissue

Every tissue type is characterized by proton density (PD) (number of protons in a voxel), T1 relaxation time and T2 relaxation time (McRobbie, 2005). Through sequences, the MR signal can be sampled at different points during the relaxation process, influencing image contrast. Images exhibiting T1 contrast are termed T1-weighted images (T1w), while those emphasizing T2 contrast are referred to as T2-weighted images (T2w). Furthermore, sequence is a succession of commands executed in such a way to present us with the desired signal and image, making them suitable for diagnostic purposes by emphasizing certain tissue characteristics or pathological features. Eco time (TE), time interval between excitation and time when the signal from the center of k-space is acquired, and repetition time (TR), time between two successive excitation pulses, are sequence parameters that have the most influence on image weighting, which can be changed by the operator. Weighting of the image is manipulation of the magnetization so that the properties PD, T1 and T2 are reflected differently depending on the image we want to acquire. Short TR provides better contrast and a lower signal-to-noise ratio, and a longer TE results in a lower signal-to-noise ratio (Huettel et al., 2008). In case of discriminating between pathologies, it is possible to use a contrast agent (e.g. gadolinium) to improve the specificity of the MRI by providing extra weighting. Other properties, magnetic resonance can be sensitive to include water diffusion mechanisms, magnetization transfer, blood oxygenation, tissue perfusion, blood vessels, and metabolism (Tsougos, 2018).

2.6 Functional Magnetic Resonance Imaging

Functional magnetic resonance imaging (fMRI), a neuroimaging procedure performed in the MRI scanner, is sensitive to blood flow changes in the brain present during the exposure to specific stimuli or even at rest. Moreover, the blood flow changes are associated with the functional brain activity, albeit indirectly (Tsougos, 2018). Strengths of fMRI include high spatial resolution, availability in both clinics and academic research and noninvasiveness of the method (Glover, 2011). Majority of the limitations stem from the fact fMRI isn't a direct measurement of neuronal activity, as well as the amount of noise present from the environment and physiology. Functional magnetic resonance imaging has seen growing utilization in clinical settings, although its origins lie predominantly in research. Initially employed to map brain activity elicited by specific stimuli or tasks (including sensory, motor, cognitive, and emotional functions) in healthy subjects, its scope has expanded to encompass the study of neurobehavioral disorders such as Alzheimer's disease, epilepsy, traumatic brain injury, and brain tumors. Notably, in the context of tumor pathology, fMRI has emerged as a well-established clinical tool, particularly for pre-surgical mapping purposes (Tsougos, 2018).

2.6.1 Principles of Functional Magnetic Resonance Imaging

Brain function requires a lot of energy, consumption of which functional MRI measures via the rate of oxygen consumption utilizing the blood oxygenation level-dependent (BOLD) signal, a measure used in functional magnetic resonance imaging (fMRI) to detect changes in brain activity. The oxygen necessary is delivered in the blood, following the premise that high energy required results in high oxygen delivery and increased blood flow. An important role is played by an iron-containing metalloprotein in the blood cells that acts as oxygen transporter, called Hemoglobin (Hb). It is possible to distinguish paramagnetic deoxyhemoglobin, when no oxygen is bound to the hemoglobin, and diamagnetic oxyhemoglobin, when oxygen is bound to the hemoglobin. The paramagnetic properties of deoxyhemoglobin cause alterations in the local magnetic fields, which in turn causes dephasing of protons due to less uniformity in the magnetic field, reducing the transverse relaxation constant T2* and increasing the decaying of the signal (Tsougos, 2018). T2* relaxation times can be directly related to the amount of iron present (Ghadery et al., 2015). Diamagnetic oxyhemoglobin causes a more uniform magnetic field, increasing the MRI signal. When there is an activation cells will consume more oxygen increasing the deoxyhemoglobin and decreasing the amount of MR signal. Furthermore, the implications

extend beyond this point. Increase in consumption of oxygen is compensated by an increase in oxygen-rich arterial blood flow, causing an increase in oxyhemoglobin amount, that is, at the capillary level, much larger compared to the amount of deoxyhemoglobin (Tsougos, 2018). Illustrations for the BOLD effect in fMRI can be seen in the figure 2.4 below.

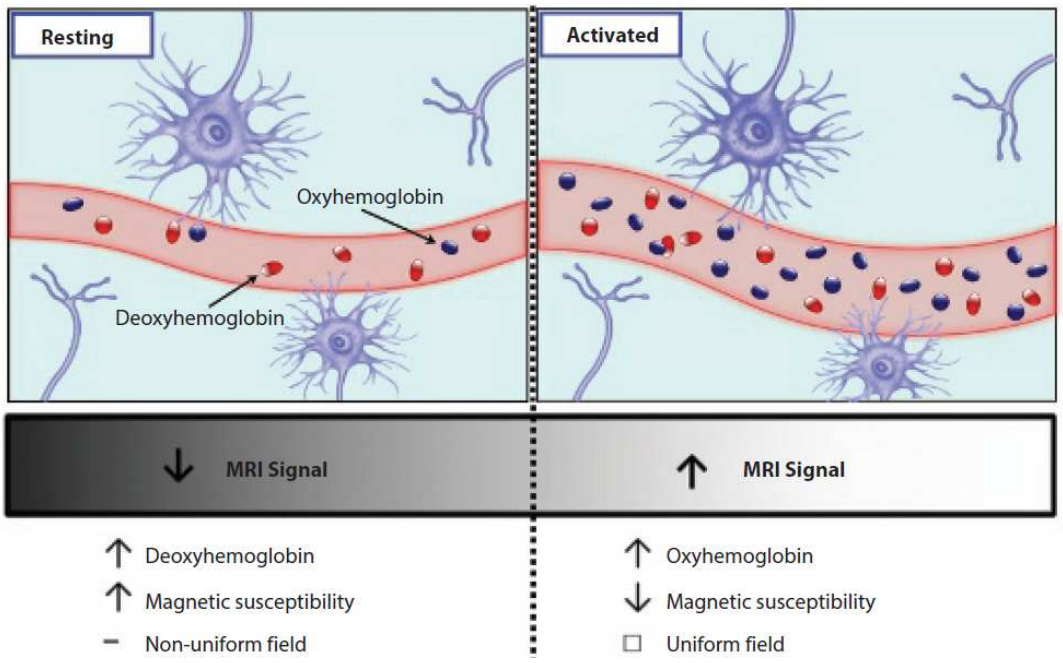

Figure 2.4 Illustration of BOLD effect in functional MR. When an activity is present, cells consume oxygen, increasing the amount of deoxyhemoglobin in the blood. Following this there is an increase in arterial blood flow in order to compensate for this consumption, leading to an increase in oxyhemoglobin (Tsougos,2018).

Hemodynamic response provides the delivery of blood to active neuronal tissues. Hemodynamic response function (HRF) is a mathematical transfer function of neuronal activity and BOLD signal, that is dependent on cerebrovascular reactivity and neurovascular coupling (Rangaprakash et al., 2018) that can provide some information about the characteristic pattern of changes in blood flow, blood volume, and oxygenation that occur in response to neuronal activity in the brain. Particularly in that sense, BOLD signal's hemodynamic response encompasses multiple subsequent stages. These stages typically follows a well-defined temporal profile, which includes an initial dip that can be explained as a transient decrease in the level of oxygenated hemoglobin (oxyhemoglobin) and an increase in the level of deoxygenated hemoglobin (deoxyhemoglobin) after a neuronal activity. This initial dip is thought to be related to increased oxygen consumption by activated neurons (Voss, 2016) . Then, following the initial dip, there is a rapid increase in blood flow, leading to an overshoot in the level of oxyhemoglobin and an increase in blood volume in the

activated region. After the positive peak, there is a period of relative undershoot, during which blood flow and oxygenation levels dip below baseline levels (Rangaprakashet al.,2021). Therefore, it is important to note that modeling the HRF to estimate neural activity from observed changes in BOLD signals in fMRI studies can be useful to understand and identify abnormalities in neurovascular dynamics, which may be indicative of neurological disorders. BOLD hemodynamic response includes a series of stages. Firstly, an initial decrease for the duration of 1 second is attributed to a transient increase in the amount of deoxyhemoglobin. Following is an increase in neuronal activity relative to baseline levels, observed to result in an increased hemoglobin blood flow. Due to the delivery of more oxygen than originally extracted from a certain brain area result in a reduction of the deoxyhemoglobin amount. The signal rises to a maximum value as a peak of hemodynamic response. If neuronal activity stretches over a prolonged period of time, the peak may similarly expand to a plateau and is typically maintained at a slightly below the peak. Following the stop of neuronal activity, the amplitude of the BOLD signal plummets below the baseline where it remains for an extended period of time. This effect is titled the post stimulus undershoot (Huettel et al., 2014).

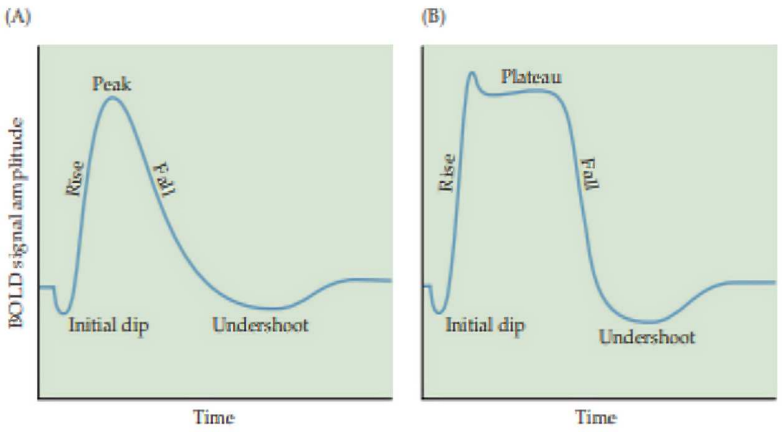

Figure 2.5 Illustration of the BOLD hemodynamic response to a (A) single short event and (B) multiple sequential blocks of events (Huettel et al., 2014).

2.6.2 Experimental design

Experiments, fMRI or otherwise, are based on an intervention in a system and observing how this intervention modulates the system response (Amaro & Barker, 2006). Main aim is to design a task which accurately tests a specific hypothesis about a certain mental process.

In functional magnetic resonance imaging (fMRI) research, different experimental designs are employed to investigate brain function and cognitive processes. Three common types of experimental designs used in fMRI studies are block design, event-related design, and mixed design (Figure 2.6) (Tsougos, 2018). Moreover, in a block design, by alternating between presenting a sequence of stimuli within a condition and epochs with a different condition, cognitive engagement in a task can be ensured. Two epochs of each condition represent a cycle (Figure 2.6 a). However there are some limitations that should be keep in mind including the inability to distinguish between correct and error trials, no regards for transient responses of the beginning and end of the task, possibility of opposite responses being summed in a single block, averaging the overall response and decreasing the magnitude of responses (Tsougos, 2018). On the other hand, the event-related design encompasses different condition trials that are presented in random sequences and not grouped in blocks, with sufficient time between different responses called inter stimulus interval. Compared to block designs, event-related designs allow avoidance of cognitive adaptation by adjusting the inter stimulus interval (Tsougos, 2018). Additionally, it is less sensitive to head motion artifacts, can be used to assess practice and allows for randomization of the order of conditions (Amaro & Barker, 2006). In that sense, it can be said that block designs are better at detecting an activation when we desire to conclude if a region is active or not, and event-related designs are better at characterizing the time course of activation when we are interested in more detailed characteristics of the neuronal response to the cognitive manipulation (Chen & Glover, 2015). Another common type of design is the mixed designs which have characteristics of both block design, in regard to the measurement of repetitive sets of stimuli, and event-related designs, in regards to the transient responses detected. Mixed designs allow for understanding of ‘what’ the role of a certain node of a network is subsiding a task (Amaro & Barker, 2006).

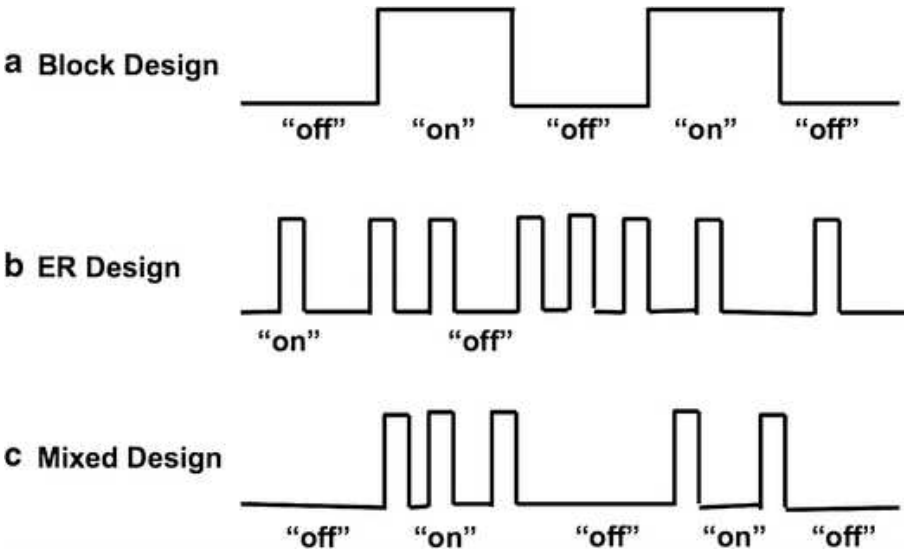

Figure 2.6. Illustration of (a)Block design, (b) Event-Related (ER) design and (c) Mixed design. The "on" and "off" levels indicate that the stimulus is either presented for an experimental or a control condition (Chen & Glover, 2015).

An alternative study design is resting-state design, where a participant lays inside an MRI scanner while not performing any tasks, allowing us to observe BOLD signal changes related to spontaneous activity (Amaro & Barker, 2006). The acquisition of the data is similar to that of event-related studies. This design relies heavily on the performance of each individual, as well as the variability between participants, the frequency of events per condition, and consequently, the statistical power of the study is largely uncertain beforehand (Chen & Glover, 2015).

3. Dynamic Causal Modeling for fMRI

3.1 Brain connectivity

Neurons do not operate autonomously, but rather function within intricate networks and systems, where their activities are influenced by broader neural circuits. They interact with other neurons and neural populations in an organized way through their afferent and efferent connections, giving rise to the ability to perform a plethora of different sensorimotor and cognitive tasks (Horowitz, 2003). Understanding brain connectivity is fundamental to unraveling the mechanisms by which neurons and neural networks encode and process information. Connectivity profoundly influences neural activity and, consequently, neural coding (Sporns, 2007). The umbrella term 'brain connectivity' encompasses:

-Anatomical connectivity defined as the pattern of anatomical connections among distinct units within a nervous system (e.g. synapses, fiber pathways),

-Functional connectivity defined as the pattern of statistical dependencies among distinct units within a nervous system,

-Effective connectivity defined as the pattern of causal interactions among distinct units within a nervous system.

According to Rykhlevskaia et al. (2008) these three connectivity types are closely related to each other. In that sense, possible measures depend on the type of connectivity. Until the development of in vivo imaging techniques, it was impossible to measure white matter integrity necessary to understand structural connectivity, which is why until that point research has been done using histological methods in animals. Results of these studies were hard to translate to humans. At this point in time, Diffusion Tensor Imaging (DTI) is the most commonly used MR technology for describing structural connectivity. On the other hand, due to its basis on brain activity, there are multiple viable options to measure functional connectivity including such as Positron Emission Tomography (PET), Functional Magnetic Resonance Imaging (fMRI), Electroencephalography (EEG), Magnetoencephalography (MEG) and event-related optical signal (EROS) (Rykhlevskaia et al., 2008). In the context of effective connectivity, various methods including the Dynamic Causal Modeling (Friston et al., 2003) proposed to investigate causal interactions between brain activities in different regions of interest obtained by the fMRI data. The choice of method depends on factors such

as the experimental design, the nature of the data, and the specific research questions being addressed. Furthermore, Dynamic Causal Modeling (DCM) for fMRI data is considered a powerful approach to analyze effective connectivity in terms of activation between brain regions of interest (Stephan & Friston, 2010). An example illustration explaining the different connectivity modalities can be seen in the figure 3.1 below.

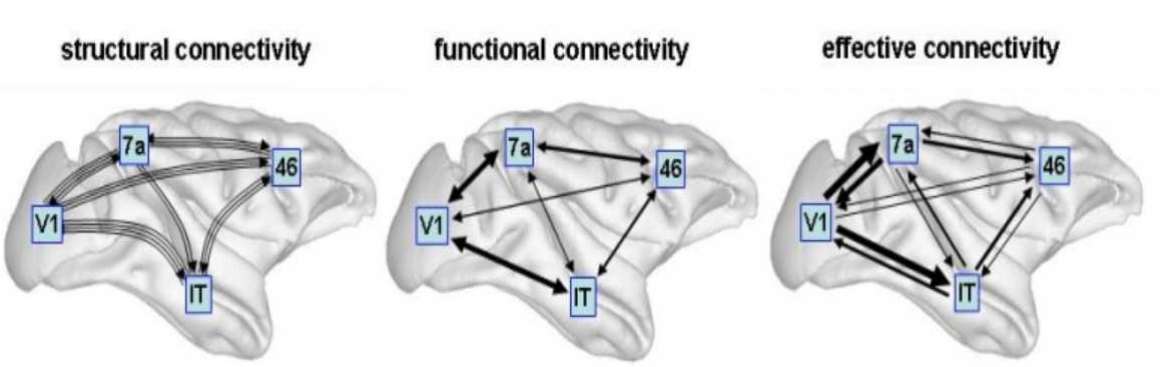

Figure 3.1. Illustration of different modalities of brain connectivity, namely structural connectivity (i.e., fiber pathways), functional connectivity (ie., correlations), and effective connectivity (i.e., information flow) among four brain regions in macaque cortex (Sporns, 2007).

3.2 Conceptual basis of Dynamic Causal Modeling

Dynamic causal modeling (DCM) is a generic approach allowing inference of hidden (unobserved) neuronal states from measured brain activity, first introduced in 2003 for fMRI data through Statistical Parametric Mapping (SPM) software (Stephan et al., 2010). Direct observation of hidden neuronal states via fMRI remains unattainable, nevertheless, yet successful modeling endeavors are. Friston and colleagues (2003) posit that DCM is based on the idea that the brain is a deterministic nonlinear dynamic system that receives inputs m and produces outputs l. In addition, Stephan and colleagues (2010) defined five key features of DCM. Firstly, DCM is based on differential equations for describing neuronal dynamics. Next, DCM is causal, based on the fact they describe how dynamics in one neuronal population cause dynamics in another neuronal population, and the influence endogenous brain activity, as well as experimental manipulations, have on these interactions. Thirdly, DCM wants to achieve neurophysiological interpretability. Fourthly, DCM uses a forward model to be able to link the modeled neuronal dynamics and specific features of measured data. Lastly, DCM is based on the Bayesian model which uses principles of Bayesian statistics to infer and compare models of brain connectivity.

DCM is used to test a specific hypothesis, based on which the experimental design is made (Friston et al., 2003). Therefore, data sets acquired in absence of experimental control, like in resting state fMRI, are not suitable. It is necessary for the DCM to have a relation to the experimental design, which in fMRI is established by an initial analysis using conventional SPM based on general linear model (GLM) (Stephan et al., 2010). GLM is a statistical framework commonly used in functional magnetic resonance imaging (fMRI) analysis to estimate and test neural activity related to experimental conditions or tasks. The GLM models the relationship between the observed fMRI data and the experimental design by representing the fMRI time series as a linear combination of explanatory variables (Monti, 2011).

DCM serves as a computational approach for specifying models of effective connectivity, which encompasses the bidirected causal influences among brain regions, essentially representing how one region affects another. These models facilitate the estimation of connectivity parameters and the testing of hypotheses. Effective connectivity, typically not directly observable, necessitates the use of models that span various spatial and temporal scales. These scales include the microscopic activity of neural populations, the meso- or

macroscopic resolution of measurements, and population-level effects suitable for characterizing individual subjects (Zeidman et al., 2019a).

Model of effective connectivity can be represented in the equation 3.1 as:

$$\dot{z} = F(z,u,\theta)$$

(3.1)

Where z represents neuronal states, F is a nonlinear function describing the neurophysiological influences that activity z in all l brain regions and inputs u exert upon changes in the others. Θ are the parameters of the model whose posterior density is required for inference. The ż represents activity state change over time, mathematically represented in the equation 3.2 as:

$$\dot{z} = \frac{dz}{dt} = f(z, u)$$

(3.2)

Specifically, the bilinear form of equation 3.1. can be notated as in the equation 3.3:

$$\begin{aligned}
\dot{z} &\approx Az + \sum u_j B^j z + Cu \\
&= (A + \sum u_j B^j) z + Cu \\
A &= \frac{\partial F}{\partial z} = \frac{\partial \dot{z}}{\partial z} \\
B^j &= \frac{\partial^2 F}{\partial z \partial u_j} = \frac{\partial}{\partial u_j} \frac{\partial \dot{z}}{\partial z} \\
C &= \frac{\partial F}{\partial u}.
\end{aligned}$$

(3.3)

Vectors Θ, in the equation 3.3., are expressed through matrices A, B and C. Matrix A represents a set of 'exogenous connections', which specify regions that are connected and whether these connections are uni- or bidirectional. Matrix B represents a set of modulatory connections, B^j, that specify which intrinsic connections can be changed by which inputs. Because B^j are second-order derivatives they are referred to as bilinear. Matrix C specifies which inputs are connected to which regions (Penny et al., 2010).

Transitioning from neuronal activity to fMRI activity by an extended version of a DCM hemodynamic model, called "Balloon model" originally introduced by Buxton and colleagues (1997) in order to reveal the coupling dynamics between neural activity and BOLD responses. The "Balloon model" describes the causal mechanisms within a hemodynamic process in a certain region of interest (ROI) during brain activation (Zhang et al., 2016).The changes in neural activity elicit a vasodilatory signal that leads to increases in blood flow and subsequently to changes in blood volume and deoxyhemoglobin content. The predicted BOLD signal is a non-linear function of blood volume and deoxyhemoglobin content (Marreiros et al., 2010). This model elaborates on how neuronal activity changes give rise to changes in blood oxygenation measured in fMRI. It involves a set of hemodynamic state variables, state equations and hemodynamic parameters (Penny et al., 2010).

The BOLD signal can be seen as a measurable (or observed) variable y of the neural activity z which we are not able to measure using fMRI, indicating the neural activity as an example of a "hidden neuronal state variable" (Kahan & Foltynie, 2013). The predicted BOLD signal is a nonlinear function of blood volume and deoxyhemoglobin content (Marreiros et al., 2010). In formula 3.4 Marreiros and colleagues (2010) elaborate that for any given combination of parameters Θ and inputs u, the measured BOLD response y is modeled as the predicted BOLD signal (the generalized convolution of inputs $F(z,u,\theta)$) together with a linear mixture of confounds $X\beta$ and Gaussian observation error ϵ.

$$y=F(z,u,\theta)+X\beta+\epsilon \tag{3.4}$$

Figure 3.2 illustrates how experimental manipulation directly perturbed neural activity. Connections presented are either extrinsic (between different regions) or intrinsic (within region; self-connections).

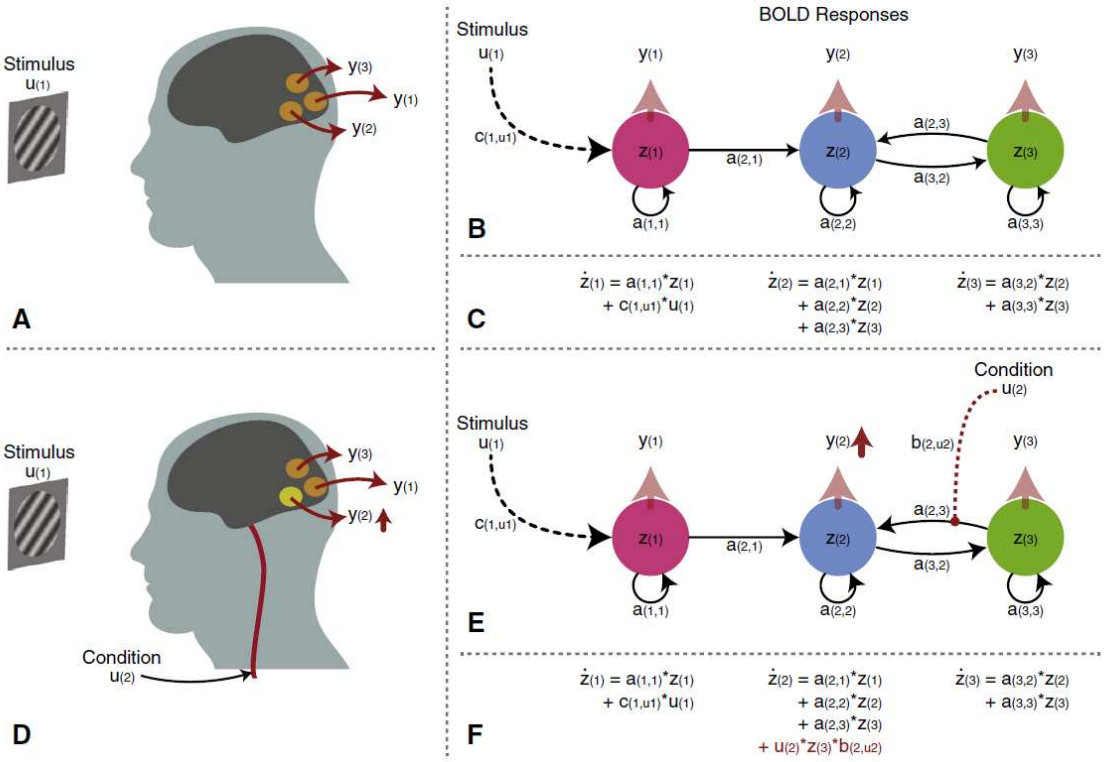

Figure 3.2 Illustrates a fMRI experiment with two different experimental manipulations. (A) The BOLD signal from three hypothetical brain regions is represented by y(1), y(2) and y(3). (B) The BOLD signal from a single region is produced by a change in its underlying neural activity z. The underlying neural activity of region 1 has an effect on the underlying neural activity of region 2 (an extrinsic connection), the strength of which is determined by the value a(2,1). The underlying activity of region 1 also has some self-inhibitory dynamics (intrinsic connection), determined by the value a(1,1). (C) Shows the rate of change of each of the regions' underlying neural activity, ż. (D) This is modeled as a modulatory input having an effect on the strength of the extrinsic connection a(2,3) (E). The strength of this effect is determined by the value b(2,u2). (F) The equations changed to accommodate the additional modulatory input (Kahan & Foltynie, 2013).

3.3 Bayesian Model Selection and Estimation

Bayesian model selection and estimation are statistical techniques used to identify the most appropriate model among a set of candidate models and estimate the parameters of the chosen model based on observed data (Stephan et al., 2010). These techniques are rooted in Bayesian statistics, which provides a framework for quantifying uncertainty and updating beliefs about model parameters and hypotheses. DCM facilitates two primary types of inference, contingent upon the research focus.

Bayesian model selection (BMS) is a powerful method which determines which among the competing hypotheses is the most likely to constitute the mechanism that generates the observed data. Specifically, for DCM BMS is used to discern among different system architectures. DCM relies on using differential equations for biophysical modeling and Bayesian statistical methods for model inversion (parameter estimation) and comparison (Marreiros et al., 2010). Bayesian estimation provides estimates of two quantities. The first being the posterior distribution over model parameters $p(\theta|m,y)$ allowing for inferences about model parameters θ. The second is model evidence, the probability of observing the data y in the model m (Friston et al., 2003). Model comparison and selection derives from the model evidence $p(y|m)$ (Marreiros et al., 2010). The model evidence can be presented as:

$$p(y|m)=\int p(y|\theta,m)p(\theta|m)d\theta \tag{3.5}$$

Firstly, if we were interested in the neurophysiological mechanisms encoded by specific parameters in a given model, we need inference on model parameters. Alternatively, if our inquiry pertains to broader aspects of model structure rather than specific model parameters, we require inference on the model space. In both cases we need Bayesian Model Selection (BMS), with the slight difference that for inference on model space BMS is sufficient, and for inference on model parameters BMS is required even when we are interested in values of model parameters and not model structure. When doing a single-subject analysis, simply evaluate the posterior density of the parameter of interest, comparing the probability with some threshold. The choice between fixed effects (FFX) and random effects (RFX) in population-based analyses depends on the treatment of parameters of interest.

In BMS, models are usually compared via the ratio of their respective evidence (Bayesian factor) or via their difference in log-evidence (relative log-evidence) (Stephan et al., 2010).

The (negative) free-energy *F*, handles posterior and priors' dependencies, while being an objective function optimized during model inversion (parameter estimation) in DCM (Marreiros et al., 2010). The (negative) free-energy F is widely used in neuroimaging and mostly preferred in DCM studies (Penny et al., 2010). Variational Laplace or Model inversion (parameter estimation) uses a Bayesian scheme, with empirical priors for the hemodynamic parameters and zero-mean shrinkage priors for the coupling parameters (Stephan et al., 2008). Inversion of a DCM constitutes minimizing the (negative) free energy F in order to maximize the model evidence or marginal likelihood. The primary objective is to identify the most appropriate model rather than focusing solely on parameter inference. In fMRI, BMS has consistently been used to choose among competing DCMs (Marreiros et al., 2010).

3.4 Bayesian Parameter Averaging and Bayesian Model Averaging

Bayesian Parameter Averaging (BPA) and Bayesian Model Averaging (BMA) are two related Bayesian statistical techniques used in model selection and estimation. Bayesian Parameter Averaging (BPA) focuses on averaging parameter estimates across multiple models, while Bayesian Model Averaging (BMA) focuses on averaging predictions or inferences across multiple models. Both techniques provide a principled framework for integrating information from multiple models and accounting for uncertainty in model selection, leading to more robust and reliable results. While they share similarities, they differ in their focus and application. Analysis of parameter estimates across the group is based on whether the mechanisms encoded by the model parameters of interest in the population can be found as fixed or random effects. When talking about basic physiological properties that do not differ between sampled subjects (fixed effects) we can consider Bayesian parameter averaging (BPA) as a likely alternative method. BPA is able to compute a joint posterior density of the whole group by combining posterior densities of each individual, in such a way, that posterior of one individual is considered the priori of another (Stephan et al., 2010).

When talking about random effects, subject specific maximum a posteriori (MAP) estimates should be entered into a second-level frequentist test (e.g. t-test or ANOVA). Alternatively, it is possible to use Bayesian Model Averaging (BMA), which utilizes the whole model space or an optimal family of models to be able to compute weighted averages of each model parameter. Weighting is provided by the posterior probability for each model. BMA is useful when none of the models outperform each other, or when comparing parameter estimates between different groups for which BMS indicates group differences with regard to the optimal model. It is crucial to correct for multiple comparisons when testing hypotheses regarding multiple comparisons (Stephan et al., 2010). Figure 3.3 summarizes the sequence of data analysis steps based on the type of inference obtained.

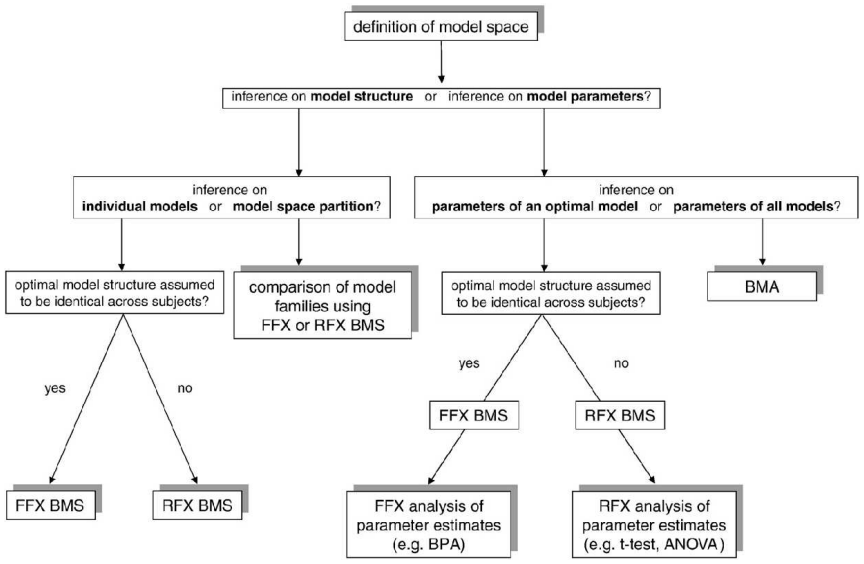

Figure 3.3. Illustrates typical sequence of analysis in DCM with consideration of the research question. FFX= fixed effects, RFX= random effects, BMS=Bayesian Model Selection, BMA= Bayesian Model Averaging, ANOVA= analysis of variance (Stephan et al., 2010).

3.5 Subject level analysis

Considering that DCM is a hypothesis-driven approach, it is paramount for the successful results that experiment design is adequate. It is necessary for the hypotheses to be clearly articulated, in connection with the effects at the within-subject level, the between-subject level, or both. We can deem the DCM forward (generative) model as a procedure which generates neuroimaging time series from underlying causes such as neural fluctuations and connection strengths. These time series are contingent upon the model's parameters (Zeidman et al., 2019a). An effective within-subject design usually encompasses the independent variation of at least two separate experimental factors. Typically, one factor involves altering the stimuli that drive neural responses, while the other factor involves adjusting the task demands or context that modulate these responses (Figure 3.4) (Zeidman et al., 2019a).

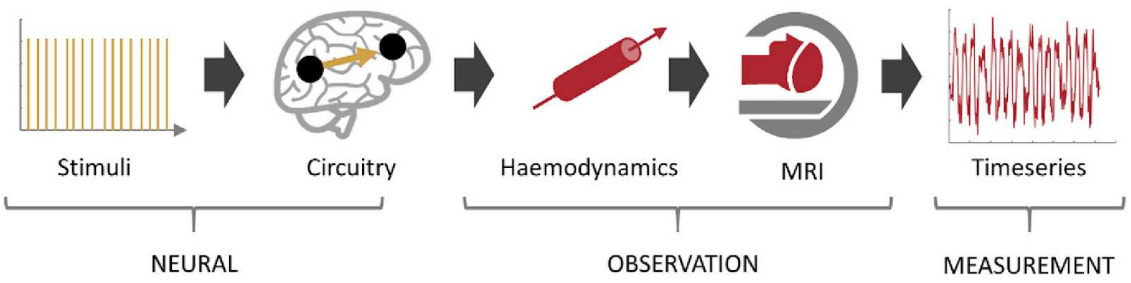

Figure 3.4. Illustrates a forward model in DCM for fMRI which encompasses the neural, observation and measurement segments. Neural model is driven by experimental stimuli, resulting in neural activity which causes a hemodynamic change in blood flow mediated by neurovascular coupling. Finally, BOLD signal is generated. By adding the observation noise we get the fMRI time series (Zeidman et al., 2019a).

To elaborate further, formula 3.6. can be interpreted as parameters controlling the region's excitatory-inhibitory balance, mediated by the interaction of the pyramidal cells and inhibitory interneurons. These parameters are negative and prevent run-away excitation in the network, a phenomenon in neural systems where neural activity becomes excessively amplified, leading to uncontrolled and potentially harmful levels of excitation. It is implemented via a necessary divide of the average connectivity matrix A and modulatory input matrices $B^{(k)}$ into two parts: intrinsic within-region self-inhibition (A_I, B_I) and extrinsic between region connectivity (A_E, B_E) where -0.5Hz is the default strength of the self-connections (Zeidman et al., 2019a).

$$\boldsymbol{J} = \underbrace{-0.5 \cdot \exp(\boldsymbol{A_I}) \cdot \exp\left(\sum_k \boldsymbol{B_I^{(k)}}\, \boldsymbol{u_k}(t)\right)}_{Intrinsic\ (self-inhibition)} + \underbrace{\left(\boldsymbol{A_E} + \sum_k \boldsymbol{B_E^{(k)}}\, \boldsymbol{u_k}(t)\right)}_{Extrinsic\ (between-region)}$$

(3.6.)

Once a forward model is specified, data simulation is possible under various models (e.g. with distinct connectivity architectures), establishing which simulation best characterizes the observed data. This process unfolds in two stages:

1) Model inversion (i.e., estimation) allows for choosing the parameters that offer the best trade-off between the model accuracy and the complexity, which is quantified by the model evidence
2) Hypotheses can be tested through the comparison of the evidence across different models with varying network architectures, both at the single-subject or group level.

The first level analysis incorporates neural responses at the within-subject level. Following model specification, next step entails acquisition of a full forward generative model, encompassing neural, hemodynamic, and noise contributions. Consequently, the selected models are specified, fitted, and deemed suitable at the single subject level (Zeidman et al., 2019a). Figure 3.5 illustrates an example of experimental timing and timeseries from a paper by Zeidman and colleagues (2019a).

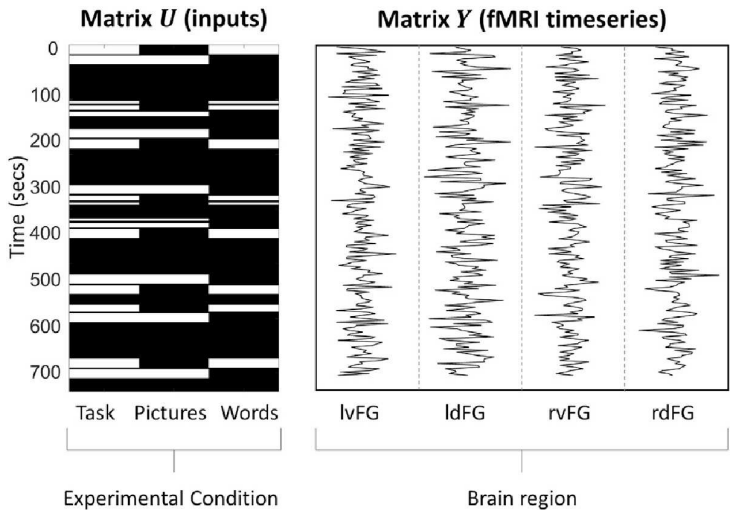

Figure 3.5 Illustration of an example of the prerequisites for DCM analysis of task fMRI data including the design (U) and data (Y). On the left in the Experimental inputs U, white areas indicate times during the experiment when experimental stimuli were shown to the subject (Zeidman et al., 2019a).

Within-subject level specifies and compares different models of evidence from different measurement techniques, to infer the neural responses of individual subjects. Following is the model parameters analysis at the second (between-subject) level, where the commonalities and differences across subjects are assessed (Zeidman et al., 2019b).

The data of each subject undergoes DCM specification and estimation of parameter probability density. Using the General Linear Model (GLM) the parameters of interest are modeled, and any unexplained between-subject variability is captured by a covariance component model. Figure 3.6 illustrates potential methods and their implementation in the SPM software via consequent Matlab functions defined in the column "Function name", as well as their description in the column "Description". For example, in Matlab (The MathWorks, Inc., 2023) using a function ***spm_dcm_specify*** allows for specification of the details of a DCM model for fMRI for a single subject, which involves defining the architecture of the neural network, specifying the experimental inputs, and setting up the parameters to be estimated or constrained within the model.

DCM for fMRI software functions in SPM.

Function name	Description
spm_dcm_specify	Creates a DCM for fMRI Matlab structure for a single subject. (Details of the DCM structure can be found in the help text of spm_dcm_estimate.m)
spm_dcm_fit	Fits (estimates or inverts) a GCM array[a] of DCMs. This in turn calls spm_dcm_estimate to fit each DCM.
spm_dcm_fmri_check	Provides basic validation statistics (e.g. explained variance) for a DCM or GCM array.
spm_dcm_fmri_priors	Specifies priors on parameters for fMRI DCMs.
spm_dcm_review	Graphical user interface for reviewing the contents of a DCM.
spm_fx_fmri	Neural and haemodynamic model for fMRI DCMs.
spm_gx_fmri	Observation model for fMRI DCMs.
spm_int	The integrator used to generate predicted timeseries from the DCM.
spm_nlsi_GN	The model estimation scheme used when fitting DCMs (variational Laplace).

Figure 3.6 Illustrates a list of MATLAB functions for SPM software utilized in DCM analysis of fMRI data (Zeidman et al., 2019a).

4. Materials & Methods

Recruitment of participants, data collection and partial image preprocessing were done for a published study by Mascheretti and colleagues (2021).

4.1 Participants

Participants were originally recruited for Mascheretti et al. (2021).

Total cohort for the existing study includes 90 subjects with 45 typical readers (TR) and 45 developmental dyslexia (DD) participants. Current study includes 2 groups of participants with the total of 40: TR group consists of 20 participants (age M=13.5, SD=1.80; 7 girls), and DD group consists of 20 participants (age M=14.1, SD=1.55; 6 girls). As the original study also investigated the genetic component of developmental dyslexia, specifically DCDC2 genetic mutation, it is taken into consideration while creating the subgroup of the current study. From the full cohort, 4 participants, 2 from the TR group and 2 from the DD group, had been selected with the genetic mutation from the overall n. of subjects of 90. DD group had a clinical diagnosis of developmental dyslexia based on The Diagnostic and Statistical Manual of Mental Disorders (DSM IV) (APA, 2006). All participants underwent neuropsychological assessments to test IQ (Wechsler, 2006), reading (Cornoldi 1995; Cornoldi, 1998; Sartori et al.,1995; Arina et al.,2013), Verbal Working Memory (VWM) (Reynolds & Bigler, 1994), phonological skills (Bartelli & Bilancia, 2006), hand preference (Briggs & Nebes, 1975) and ADHD (Conners, 1989; Conners et al., 1998; Nobile et al., 2007).

4.2 MRI Acquisition

MRI data were collected using a 3T Philips Achieva d-Stream scanner (Best, The Netherlands) equipped with a 32-channel head coil. Visual stimuli were generated using Presentation software (Neurobehavioral System Inc., Berkeley, CA, USA) and presented via a VisuaStim digital device for fMRI (Resonance Technology Inc., Northridge, CA, USA). Participants viewed the stimuli through MRI-compatible goggles featuring dual displays, operating at a frame rate of 60 Hz and spatial resolution of 800 × 600 (4/3 aspect ratio), subtending a horizontal visual angle of 30 degrees. Responses and reaction times were recorded using an MRI-compatible pad. The MRI protocol included acquisition of a T1-weighted anatomical scan using a 3D Turbo Field Echo sequence, serving as a

morphological reference (Field Of View (FOV) = 256 × 256 × 175 $mm^{3,}$ voxel size = 1 × 1 × 1 $mm^{3,}$ shortest Time of Repetition (TR) (~8.1 ms), shortest Time of Echo (TE) (~3.7 ms), Flip Angle (FA) = 8 degrees). Functional MRI (fMRI) data were acquired using a T2*-weighted Gradient Echo planar sequence (FOV = 240 × 240 mm^2, voxel size = 3 × 3 mm^2, slice thickness = 3 mm, slice gap = 0.5 mm, slice number = 39, TR = 2 s, TE = 26 ms, FA = 90 degrees).

4.3 fMRI Task Design

4.3.1 Full-field Sinusoidal Gratings

The task comprised 14-second blocks of "M stimuli" (Figure 4.1), "P stimuli" (Figure 4.2) and blank stimuli (consisting solely of a fixation point). The stimuli were specifically meant to target M- and P- pathways. The M stimulus presented as a monochrome, low spatial frequency, high temporal frequency, high luminance contrast, full-field sinusoidal grating with sinusoidal counterphase flicker. On the other hand, the P stimulus presented as a high color contrast, high spatial frequency, low temporal frequency, low luminance contrast full-field sinusoidal grating with sinusoidal counterphase flicker. Specifically, the M stimulus featured a 100% luminance contrast, black-and-white grating with a spatial frequency of 0.5 cycles per degree (cpd) and a flicker frequency of 15 Hz. On the other hand, the P stimulus comprised a low luminance contrast, high color contrast red-green grating with a spatial frequency of 2 cpd and a flicker frequency of 5 Hz. The blank stimulus presented a gray screen with mean luminance, with the outer borders of each stimulus fading into gray to prevent sharp visual edges. Both gratings were displayed at one of six orientations with orientation changes occurring every 2.33 seconds. In total there were 28 blocks (8 M, 8 P, and 12 blank) presented in pseudorandom order to ensure that the same stimulus type did not appear in adjacent blocks, thus minimizing adaptation effects. A white fixation point remained at the screen center throughout the stimulus blocks. Participants were instructed to maintain fixation during the task and performed an irrelevant target detection task during the M and P stimulus blocks to ensure they do so. The target, a bidimensional Gaussian contrast reduction patch, varied in size based on its distance from the fixation point and appeared randomly for 300 ms and in random positions 50% of the time during the second half of each stimulus block. At the end of each stimulus block, the screen turned gray, prompting participants to respond to questions regarding target appearance by pressing corresponding buttons on the response pad (i.e., right button for "Yes" and left button for "No"). Participants

had 4 seconds to provide their responses, with a 2-second inter-stimulus waiting period between stimulus blocks.

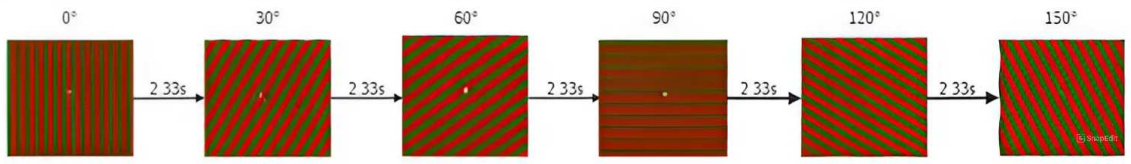

Figure 4.1 illustrates P-stimulus

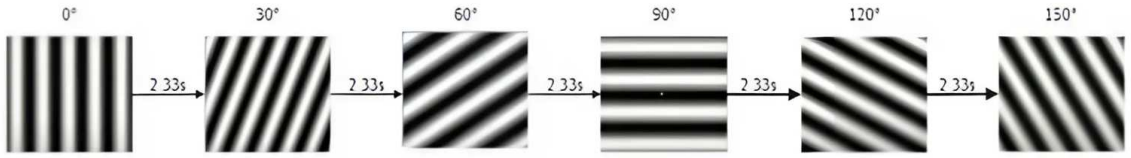

Figure 4.2 illustrates M-stimulus

4.3.2 Coherent Motion Sensitivity Detection

Sensitivity to motion coherence, with specific focus on radial motion (expanding or contracting) was performed. The stimuli consisted of 50 small white and 50 small black dots, displayed for 250 ms on a gray background. A subset of dots moved coherently at a speed of 10 degrees per second, while the remaining dots appeared randomly. Employed were three levels of coherent motion (CML: Coherent Motion Level) 6%, 15%, and 40%. At the onset of each stimulation block, a white fixation point appeared at the screen center for 0.5 s, followed by the 0.25 s coherent motion stimulus. Participants were instructed to maintain fixation throughout the task and were actively engaged in a motion detection task, responding by pressing the corresponding button on a response pad (i.e., right button for expanding motion and left button for contracting motion). After the stimulus presentation, subjects had 4 seconds to respond to the question, even if they were unable to discern the direction of motion. A 4.25-second inter-stimulus interval was introduced between stimulus blocks. The experimental protocol comprised 48 stimuli (with 8 repetitions for each combination of coherence level and motion direction), presented in a pseudorandom order so that the same coherence level could not occur in more than two consecutive blocks, regardless of the motion direction.

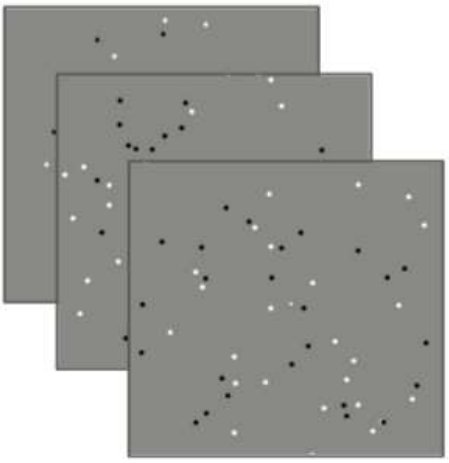

Figure 4.3 illustrates Coherent Motion stimuli

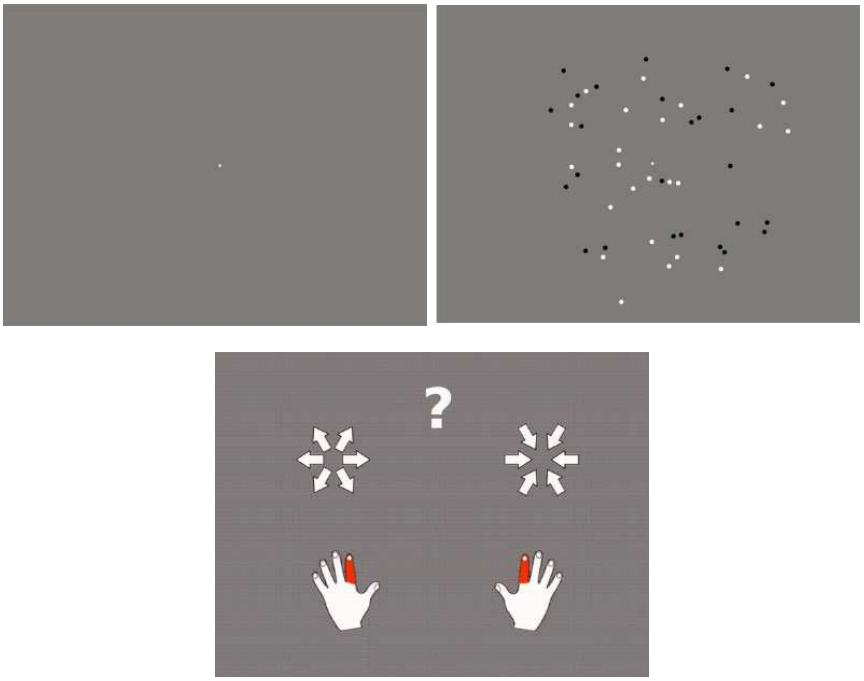

Figure 4.4 illustrates Coherent Motion fixation point and stimuli with its consequent hand response portraying the visuo-motor nature of the task.

4.4 Image Preprocessing and Analysis

Generally, prior to the statistical analysis it is necessary to do preprocessing of the functional magnetic imaging (fMRI) data. Preprocessing itself contains multiple steps to clean and standardize data for further use (Esteban et al., 2019). The preprocessing of T1-weighted structural images and fMRI data was completed via the conjoint use of well-known software packages (e.g. SPM12 and FSL). Further general elaboration on both, structural and

functional, preprocessing pipelines can be found in the following sections. For the purpose of this thesis, we used the partially preprocessed data from the study of Mascheretti et al 2021. Data acquisition, as well as the partial image preprocessing, were completed by Mascheretti and colleagues (2021) for their study, and later were shared with for the purpose of this project.

4.4.1 Structural preprocessing

4.4.1.1 BET Extraction

When conducting a fMRI study, primary focus is the brain tissue, which at the time of acquisition of the original image is not the solely present. Therefore, in order to continue the conductance of a fMRI study, it is necessary to remove all non-brain tissues, such as the neck, bone, soft tissue, the skull, as well as the background as all of these will potentially cause problems during further analysis. For this purpose Brain Extraction Tool (BET) can be used as part of the FSL package (Smith, 2002).

Depending on the specific interest of the study, variety of options can be implemented into the standard pseudo code that is generally used for BET extraction:

bet <input> <output> [options]

Among different options, most commonly used ones include:

- B – neck correction
- f - vertical gradient in fractional intensity threshold
- g - fractional intensity threshold
- c – central gravity point

Final result of the image containing only brain tissue is available for viewing and inspection in FSLeyes (McCarthy, 2024), the FSL image viewer.

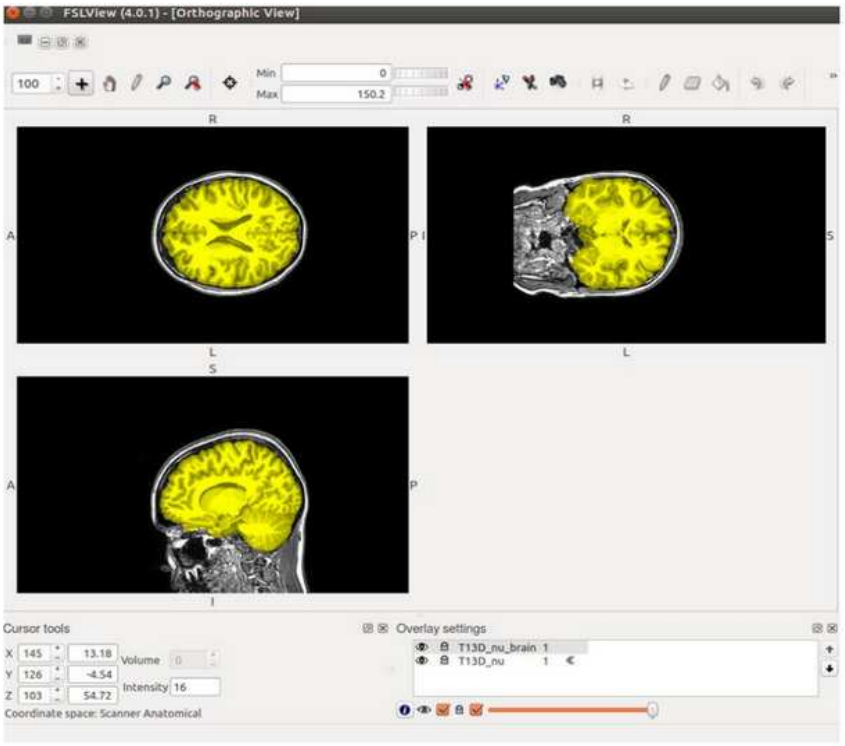

Figure 4.5 illustrates an example image of brain extraction using FSL BET (courtesy of Gökçe Korkmaz, 2022).

4.4.1.2 Segmentation

Brain has multiple different tissue types including gray matter, white matter and cerebrospinal fluid (CSF) (Dora et al., 2017). Segmentation is used to remove unwanted artifacts and transform the data into standardized format. Alternatively stated, segmentation is used to identify and classify these different tissue types, allowing us to do further analysis on a specific brain tissue type (e.g. fMRI studies can focus solely on gray matter). Segmentation can be done in SPM (Penny et al., 2011) Matlab (The MathWorks, Inc., 2023) or using FSL's FAST (FMRIB's Automated Segmentation Tool) (Zhang et al., 2001). Typically, the image extracted using BET serves as the input image for FAST. The "-o" flag is utilized to specify the base name for output images. Additionally, users can specify the number of segmented tissue types when employing FSL FAST. The default number is 3 (representing White Matter, Gray Matter, and CSF), but in cases of poor gray/white matter contrast, this can be reduced to 2. Either way, the output creates files indicating the type of matter (e.g. pve_0 for CSF, pve_1 for gray matter, and pve_2 for white matter).

The pseudo code for FSL FAST is as follows:

fast<input> <output> -o fast_segm

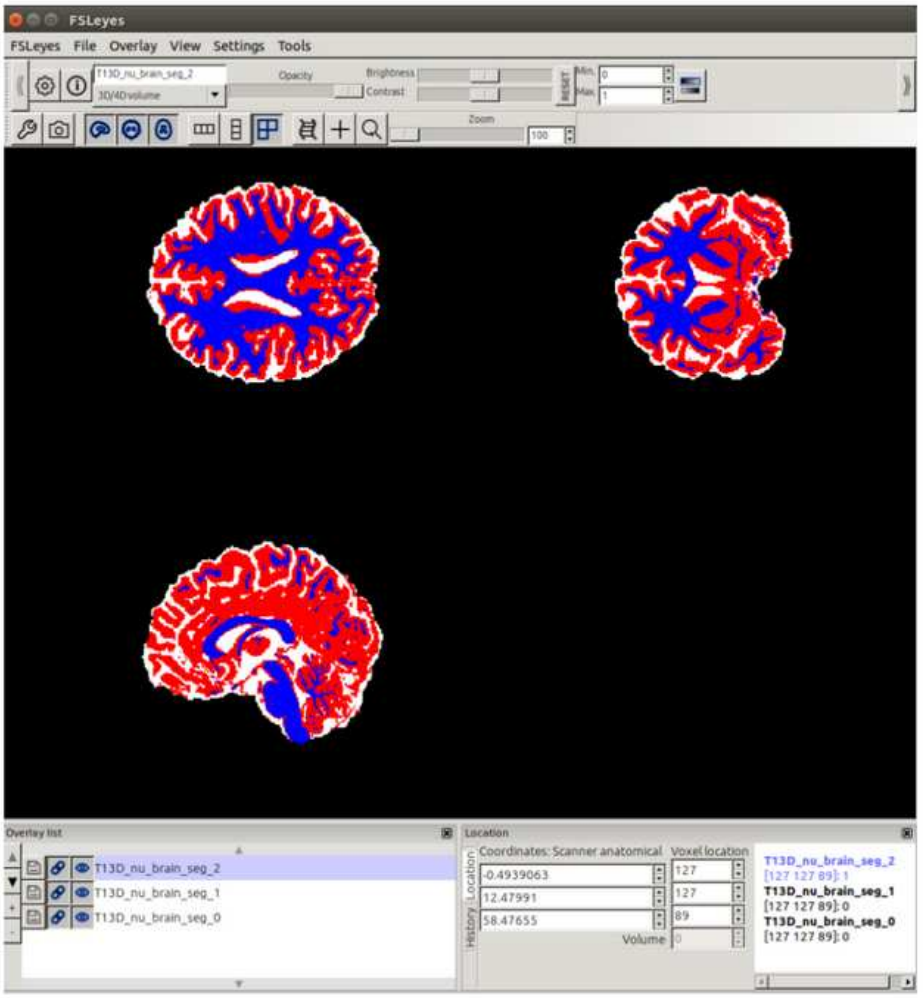

Figure 4.6 illustrates an example image of brain segmentation using FSL FAST , with red color portraying gray matter, white color portraying Cerebrospinal fluid and blue color portraying white matter(courtesy of Gökçe Korkmaz, 2022).

4.4.2 Functional preprocessing

4.4.2.1 MP-PCA

Marčenko-Pastur (MP-PCA) is used in order to delete the noise from the raw functional images. Reduction of noise is necessary in the preprocessing of MR image series. Noise corrupts MRI measurements and affects statistical analysis of functional MRI. MP-PCA addresses this problem, which cannot be solved on the hardware side due to physical limitations inherent in MR imaging, while improving signal-to-noise ratio (SNR) (Ades-Aron et al., 2018).

4.4.2.2. Slice timing

Most functional magnetic resonance image (fMRI) scans utilize echo planar imaging (EPI), a technique which rapidly captures single or multiple 2D slices and assembles them into a 3D volume. However, due to the inherent nature of fMRI acquisition, slices cannot be acquired simultaneously, resulting in temporal misalignment. To address this issue, preprocessing pipelines commonly integrate slice timing correction (STC). This step corrects for slice-dependent delays by shifting the time series of each slice, ensuring temporal alignment to a reference time-point (Parker & Razlighi, 2019).

4.4.2.3 Realignment

Head movement hugely affects the data, as the signal change in a particular voxel caused by movement may result in signals originating outside the brain. To address this issue, the procedure aims to spatially align all functional images with the initial functional image, effectively mitigating undesired participant movement during scanning. Consequently, the objective of this step is to ensure that all images are aligned such that the brain occupies a consistent position across every image, ensuring that the signal from a specific voxel consistently emanates from the same anatomical location (Zafar, et al. 2015).

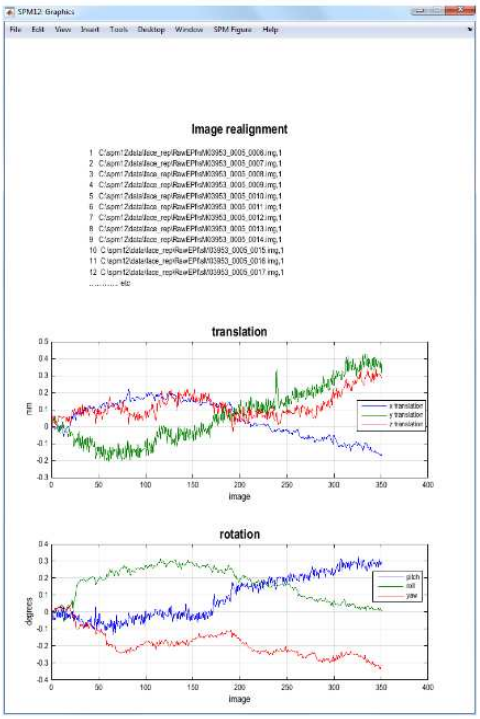

Figure 4.7 illustrates an example image of realignment (Ashburner et al., 2020)

4.4.2.4 Co-registration

With co-registration it is possible to overlay a structural (e.g. T1-weighted) with a functional (e.g. Echo planar imaging) image. Co-registration gives a better spatial image for further use in the normalization step (James et al., 2014). Co-registration can be performed by using FSL's FLIRT, and indicating the input, which refers to the image undergoing transformation, and the reference volume, which serves as the alignment target for the input. Typically, the input image corresponds to a functional scan, while the reference volume is a T1-weighted anatomical image.

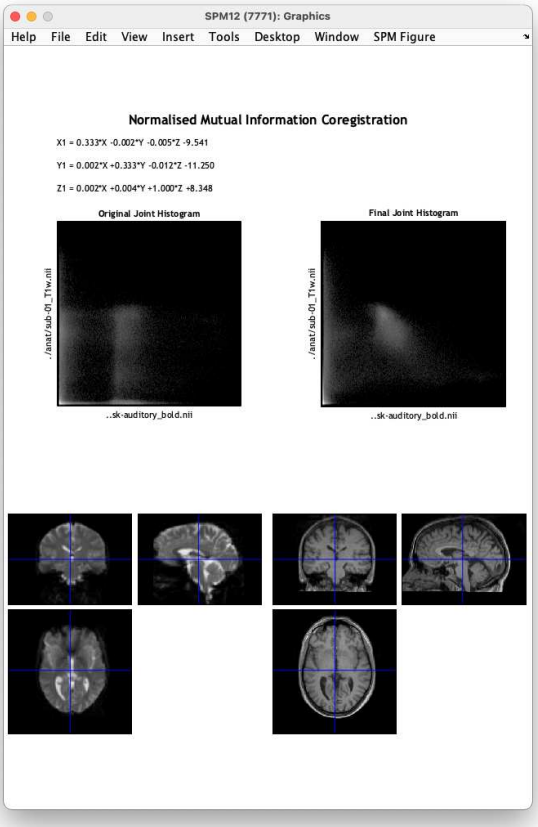

Figure 4.8 illustrates an example image of coregistration (Ashburner et al., 2020)

4.4.2.5 Quality Control with SPM's CheckReg tool

CheckReg, a tool within the SPM framework, is designed to verify the coregistration of multiple images. It assesses the alignment between a structural image and the mean of functional images obtained via fMRI and serves as a quality control measure

post-coregistration to confirm that images are accurately aligned and share the same anatomical positions, minimizing significant errors or mismatches (Ashburner et al., 2020).

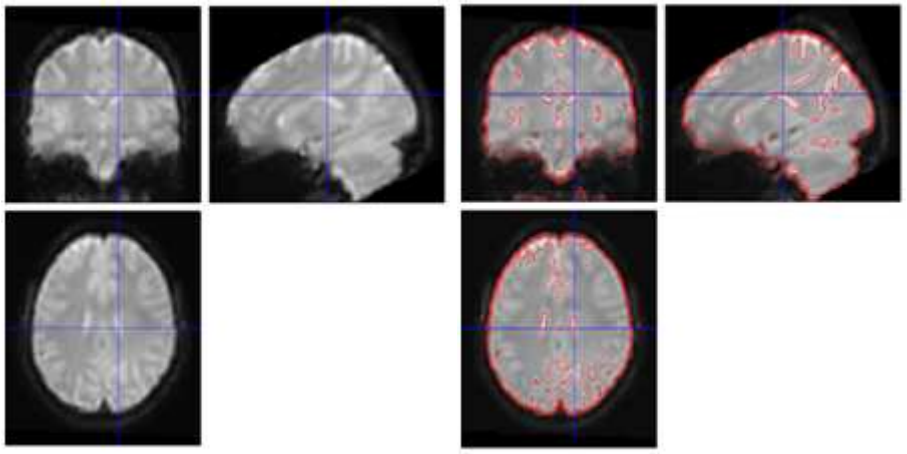

4.9 illustrates an example image of quality check with CheckReg tool

4.5 General Linear Model

Within the General Linear Model (GLM) framework, fMRI time series is modeled at each voxel through a linear combination of multiple regressors, which are defined as explanatory variables corresponding to specific experimental effects (Flandin & Penny, 2007). The statistical analysis of fMRI data employs a mass-univariate approach based on General Linear Models (GLMs), involving several key steps. Firstly, the GLM design matrix, fMRI data files, and filtering are specified. Secondly, GLM parameters are estimated using classical or Bayesian approaches. Thirdly, results are interrogated using contrast vectors to generate Statistical Parametric Maps (SPMs) or Posterior Probability Maps (PPMs). The design matrix defines the experimental design and hypothesis testing, with one row for each scan and one column for each effect or explanatory variable, such as regressors or stimulus functions. In SPM, data analysis across multiple subjects typically involves two stages: "first-level" models for within-subject analysis and "second-level" models for population-level inferences. At first-level each subjects' parameters of the model are specified and estimated. Using contrast images from each subject as summary measures of subject responses, they are entered into the second-level model. Second-level as well encompasses model specification and estimation (Ashburner et al., 2020).

In order to define a GLM it is necessary to define the conditions first. In our study, the defined conditions are Coherent-15 and Magno, representing Coherence Motion Sensitivity

task condition with 15% level of coherence which best distinguishes between the two groups (Mascheretti et al., 2021) and Full-Field Sinusoidal Grating task magnocellular condition which is based on Magnocellular theory of developmental dyslexia (e.g. Stein, 2019), respectively. Following is the definition, estimation and specification of the GLM. Once the GLM has been specified and estimated, the next step is defining a t-contrast that tests for Coherent-15 and Magno, as well as an effects of interest F-contrast used for mean-correcting the extracted time series. Further, it is necessary to extract one representative fMRI time series from each brain region of interest.

4.6 Conjunction Analysis

In fMRI studies, an effect or activation typically refers to the difference in brain activity observed between different experimental conditions, such as an activation task versus a baseline task. When utilizing the general linear model (GLM) for fMRI data analysis, various methods are available depending on the specific research question. Cognitive subtraction is employed to test for a single effect, while factorial designs are utilized to examine interactions between different experimental conditions. Conjunction analysis aims to simultaneously test for multiple effects within one subject or for the same effect across different subjects (Friston et al. 2019). The cognitive conjunction approach detects brain regions that exhibit significant overall activation (the sum of all effects) without significant differences (interactions) between individual effects, using classical test statistics (Rudert & Lohmann, 2008). Friston & Price (1997) proposed a method for interpreting a valid conjunction analysis within a brain map of activations, outlining the following criteria: 1) each voxel demonstrates significant activation by two or more tasks, 2) there is no significant modulation by interaction effects between tasks at each voxel, and 3) the estimated relationships between each voxel and each task do not exhibit significant differences.

For our study we did a Full factorial design comparing two tasks (Coherent Motion Sensitivity task and Full Field Sinusoidal Gratings task) over two groups (typical reader group and developmental dyslexia group) (Figure 4.10 and Figure 4.11).

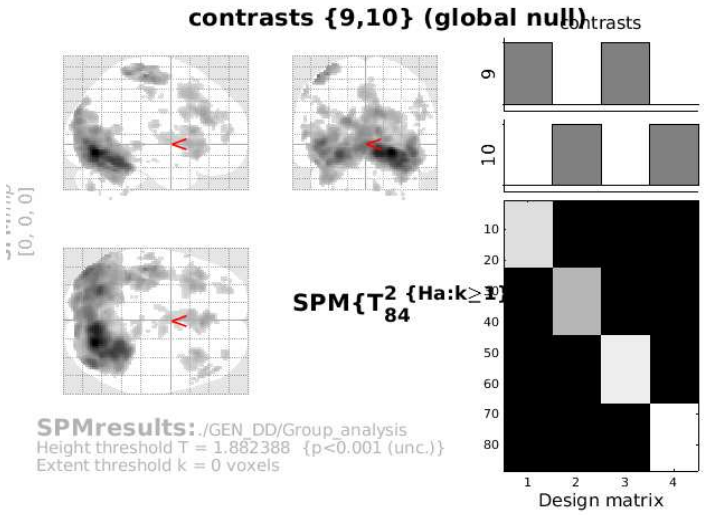

Figure 4.10 illustrates the conjunction analysis glass brain and matrix.

Statistics: ***p-values adjusted for search volume***

set-level		cluster-level				peak-level					mm	mm	mm
p	c	$p_{FWE\text{-}corr}$	$q_{FDR\text{-}corr}$	k_E	p_{uncorr}	$p_{FWE\text{-}corr}$	$q_{FDR\text{-}corr}$	T	(Z_E)	p_{uncorr}			
0.000	**48**	**0.000**	**1.000**	**13346**	**0.000**	**0.000**	**0.000**	**6.77**	**Inf**	**0.000**	**22**	**-72**	**-10**
						0.000	0.000	5.97	Inf	0.000	14	-70	-10
						0.000	0.000	5.33	7.28	0.000	32	-56	-16
		0.001	**1.000**	**537**	**0.000**	**0.000**	**0.000**	**3.95**	**5.68**	**0.000**	**-46**	**-26**	**62**
						0.001	0.001	3.73	5.42	0.000	-38	-40	64
						0.002	0.001	3.67	5.35	0.000	-46	-18	60
		0.000	**1.000**	**738**	**0.000**	**0.035**	**0.014**	**3.18**	**4.74**	**0.000**	**4**	**28**	**28**
						0.048	0.018	3.11	4.66	0.000	-2	32	22
						0.207	0.059	2.80	4.27	0.000	-2	16	44
		0.001	**1.000**	**530**	**0.000**	**0.057**	**0.020**	**3.08**	**4.62**	**0.000**	**-30**	**20**	**10**
						0.112	0.033	2.94	4.44	0.000	-30	26	-2
						0.116	0.034	2.93	4.43	0.000	-36	14	0
		0.067	**1.000**	**195**	**0.008**	**0.080**	**0.027**	**3.01**	**4.53**	**0.000**	**-40**	**26**	**28**
						0.350	0.101	2.67	4.10	0.000	-42	18	32
						0.441	0.128	2.60	4.01	0.000	-38	12	26
		0.010	**1.000**	**326**	**0.001**	**0.088**	**0.028**	**2.99**	**4.51**	**0.000**	**32**	**22**	**-10**
						0.289	0.083	2.72	4.16	0.000	38	22	-4
						0.733	0.241	2.41	3.77	0.000	40	14	-4
		0.876	**1.000**	**31**	**0.243**	**0.339**	**0.099**	**2.68**	**4.11**	**0.000**	**8**	**-76**	**-42**
		0.436	**1.000**	**82**	**0.067**	**0.422**	**0.125**	**2.62**	**4.03**	**0.000**	**48**	**40**	**24**
						0.464	0.135	2.59	3.99	0.000	48	30	38

table shows 3 local maxima more than 8.0mm apart

Height threshold: T = 1.88, p = 0.001 (1.000)
Extent threshold: k = 0 voxels
Expected voxels per cluster, <k> = 24.469
Expected number of clusters, <c> = 8.59
FWEp: 3.107, FDRp: 2.884

Degrees of freedom = [1.0, 84.0]
FWHM = 15.0 15.6 12.3 mm mm mm; 7.5 7.8 6.1 {voxels}
Volume: 1395232 = 174404 voxels = 448.1 resels
Voxel size: 2.0 2.0 2.0 mm mm mm; (resel = 359.21 voxels)
Page 1

Figure 4.11 Illustrates the conjunction analysis statistics table

4.7 VOI Extraction

Many functional MRI analyses, including DCM, start with extracting representative timeseries from selected brain regions. These are called Volumes of Interest (VOIs) or Regions of Interest (ROIs). By previously doing the conjunction analysis, deciding on VOIs was based on the overlapping activation from the two tasks performed, as well as the theoretical background. The regions investigated for each subject include right Medial Frontal Gyrus (MFG_R), left Medial Frontal Gyrus (MFG_L), right V5 (V5_R), left V5 (V5_L), right Crus I (CRUS I_R), left Crus I (CRUS I_L), bilateral V1 (V1_B).

Starting from conjunction analysis, we used three different brain atlases Harvard-Oxford cortical and subcortical structural atlas (Desikan et al., 2006; Frazier et al., 2005; Goldstein et al., 2007; Makris et al.,2006), Probabilistic cerebellar atlas (Diedrichsen et al., 2009) and Julich-Brain Cytoarchitectonic Atlas (Amunts et al., 2020). We restricted the atlas mask with the group level activation ($p<0.005$). During this procedure, it is essential to define the geometry, dimensions, and thresholds of the contrast for each relevant Region of Interest (ROI). Table 1 presents this information along with the coordinates of the ROIs at the group level. The outcome of group-level VOI extraction is the generation of group-level mask images in NIfTI format and VOI.mat files, which include details about the extracted masks. An example of an extracted time series for one VOI is shown in Figure 4.13. We did further restriction with subject specific time series extraction ($p<0.05$). During the VOI extraction for subject specific activation in the Full-field sinusoidal grating task, we encountered challenges likely due to the incompatible nature of the task causing "empty" voxels with no activation within the ROIs for most participants. Consequently, we decided to proceed only with the Coherent Motion Sensitivity task. Additionally, four subjects (S11, S18, S30, S37), two subjects from TR and two from DD group, faced similar issues and were therefore excluded from the study.

The theoretical rationale for selected brain regions is based on involvement of Ventral Attention Network (Vossel et al., 2013) and Magnocellular pathway (Stein,2019) in developmental dyslexia, as well as Cerebellar Deficit Hypothesis of developmental dyslexia (Stoodley & Stein, 2013).

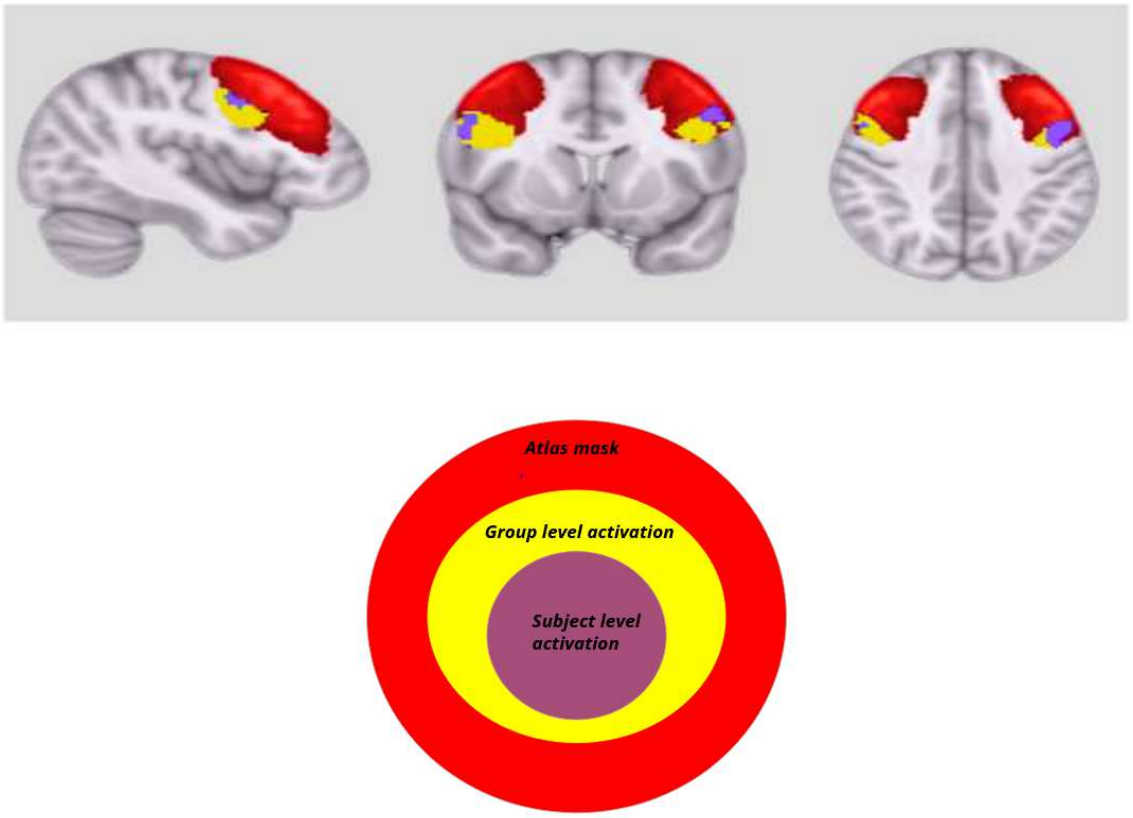

Figure 4.12 VOI extraction. On the left is a VOI extraction rationale. Red portrays Atlas mask. Yellow portrays restriction from group level activation and Purple portrays further restriction with subject level activation. On the right is a Middle Frontal Gyrus VOI extraction of a random subject

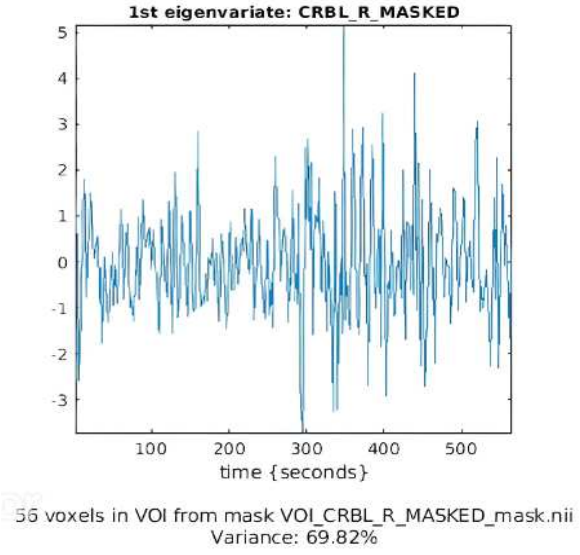

Figure 4.13 illustrates extracted time series from right Crus I

Region	Geometry	Coordinates	Threshold
MFG_R	Sphere, 15mm	[45.71 10.99 30.99]	0.005 Uncorrected
MFG_L	Sphere, 15mm	[-44.03 4.81 35.87]	0.005 Uncorrected
V5_R	Sphere, 15mm	[44.87 -66.83 3.492]	0.005 Uncorrected
V5_L	Sphere, 15mm	[-41.17 -74.15 4.95]	0.005 Uncorrected
CRUSI_R	Sphere, 10mm	[25.67 -75.48 -19.94]	0.005 Uncorrected
CRUSI_L	Sphere, 10mm	[-25.68 -72.01 -20.32]	0.005 Uncorrected
V1_BIL	Box, [50 50 50]mm	[6.99 -78.34 4.51]	0.005 Uncorrected

Table 1 Geometry selection of each ROI. MFG_R - right middle frontal gyrus, MFG_L - left middle frontal gyrus, V5_R - right middle temporal region, V5_L - left middle temporal region, CRUSI_R - right crus I of the cerebellum, CRUSI_L - left crus I of the cerebellum, V1_BIL - bilateral primary visual cortex.

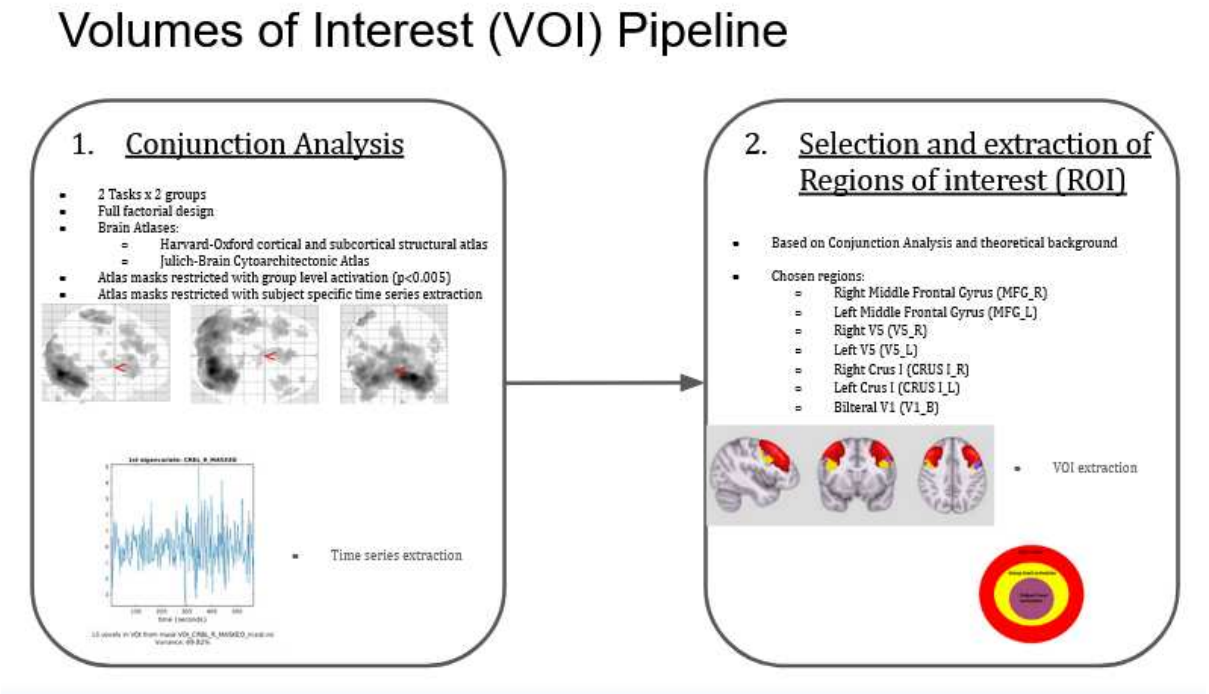

Figure 4.14 illustrates VOI extraction pipeline

4.8 Hypothesis testing

This study is exploring Dynamic Causal Modeling (DCM) analysis on fMRI data to assess effective connectivity differences in developmental dyslexia. For both developmental dyslexia and typical reader groups the same nodes of the interested brain regions, as well as among different models were used. Regions are: : MFG_R, MFG_L, V5_R, V5_L, CRUS I_R, CRUS I_L, V1_B.

Following the decision on the regions, it is important to establish the driving input, where the signal enters the system. The tasks used are attention tasks, which participants visually observed, therefore Primary Visual Cortex (V1) was selected.

Next, two different models were constructed: fully connected one and a reduced model based on the structural connectivity information between the cerebellum and the cerebrum (Palesi et al., 2015; Jobson et al., 2022). Fully connected model refers to a model where all possible connections between the regions of interest (ROIs) are included. This means that every region can potentially influence every other region, both directly and indirectly. Moreover, it does

not include any priors and connects all the regions between each other. Considering that in this case the number of connections is extremely large, it could be more sensible to introduce the reduced model to avoid possible overfitting, which consists only of the hypothesis driven connections.

As previously mentioned, we also introduced a structurally-informed reduced model, titled Cross Brain model, based on the structural connectivity to see the structurally informed effects in developmental dyslexia and typical reader groups. Based on the literature (e.g. Karavasilis et al., 2019; Pieterman et al., 2016) , the pruned connections were the ipsilateral connections from Cerebellum to Cerebrum and vice versa, as well as the connections between two cerebellar hemispheres. All the analyses described above were implemented with SPM12- MATLAB2023a. Models are illustrated in figures 4.15 and 4.16.

DCM can also be used to measure self-connectivity, which is also referred to in the literature as intrinsic or endogenous connectivity. This type of connectivity is technically defined as intra-regional connections within a given volume of interest (Friston et al., 2003). Intrinsic connections solely exert an inhibitory (negative) influence on each region included in the model. In addition, they regulate the excitatory and inhibitory extrinsic (between-region) connections that the model may estimate (Snyder et al., 2021).

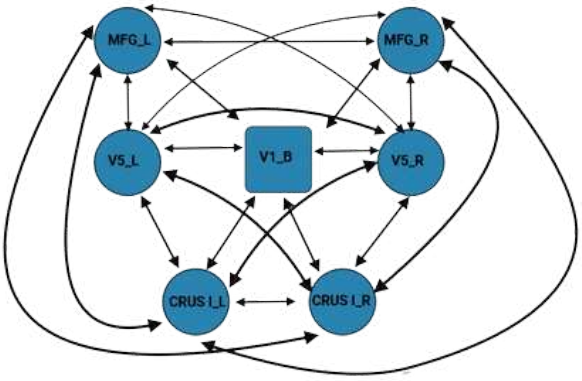

Figure 4.15 illustrates a Fully Connected model in which all the nodes are connected with each other (created in BioRender.com).

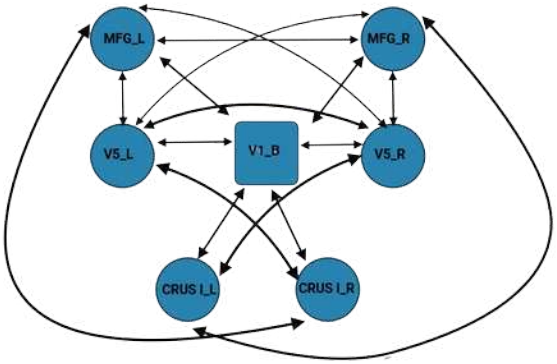

Figure 4.16 illustrates a reduced model titled Cross Brain model based on the structural connectivity. Pruned connections are between ipsilateral cerebellum and cerebrum as well as between the two cerebellar hemispheres (created in BioRender.com).

Hypothesis was tested and defined:

H: There is a difference in effective connectivity dynamics between typical readers and developmental dyslexia groups in both Fully Connected and structurally informed Cross Brain Models (Figure 4.17)

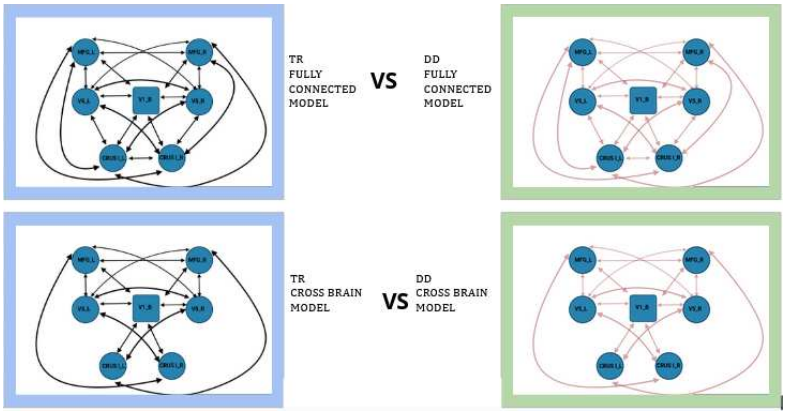

Figure 4.17 illustrates the hypothesis by comparing two groups in both models. The groups are differentiated by the color of the connections with black representing typical readers group and pink developmental dyslexia group.

4.9 Statistical Analysis

Following an estimation of each model on all subjects, both models were analyzed with Bayesian Model Averaging using a Matlab function <spm_dcm_bma> on all subjects. Results show posterior probability for each parameter of all subjects by averaging subject specific parameters. By averaging over all subjects, we obtain a comprehensive view of the parameter distributions, which reflects the variability and commonalities within the population. The same BMA analysis was repeated for both models to ensure that the results were not specific to one particular model but were robust across different theoretical frameworks. This is crucial as it validates the consistency of the findings and helps in confirming the reliability of the observed patterns.

5. Results

Implementing the pipeline described in the Methods chapter, following results are reported.

5.1 Conjunction analysis

Our conjunction contrast focused on the brain regions with higher activation associated with developmental dyslexia subjects' activation on both tasks versus corresponding healthy controls. Statistical significance was set at $p < 0.05$ without family-wise error (FWE) correction in all tests during group analysis. Overlaying the brain activity from both Coherent Motion Sensitivity task and Full-Field Sinusoidal Grating task, presented the brain activity that is consistent between tasks. The overlaying activity is present in multiple regions including right Medial Frontal Gyrus (MFG_R), left Medial Frontal Gyrus (MFG_L), right V5 (V5_R), left V5 (V5_L), right Crus I (CRUS I_R), left Crus I (CRUS I_L), bilateral V1 (V1_B). Figures 5.1, 5.2, 5.3 and 5.4 represent the glass brain and slice view with different axes images with brain activity consistent in both tasks.

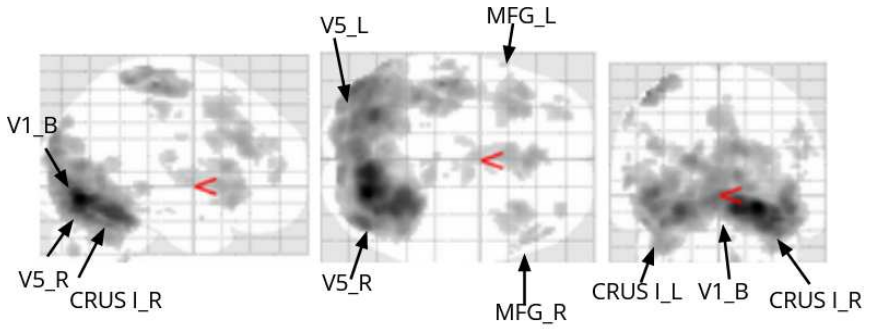

Figure 5.1 illustrates sagittal, transverse and coronal glass brain images from conjunction analysis overlaying Coherent Motion Sensitivity task and Full-Field Sinusoidal Grating task brain activities (generated by xjView 10.0.)

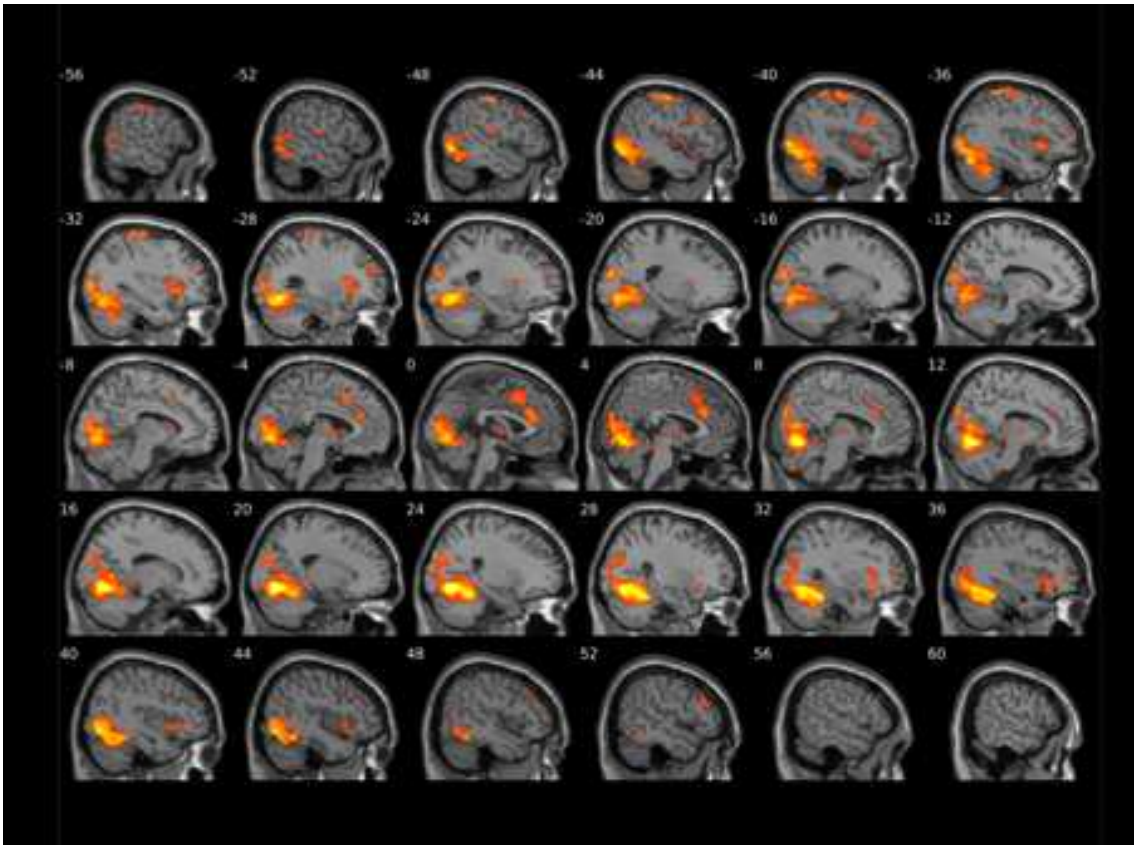

Figure 5.2 illustration of sagittal slice brain view from conjunction analysis overlaying Coherent Motion Sensitivity task and Full-Field Sinusoidal Grating task brain activities (generated by xjView 10.0.)

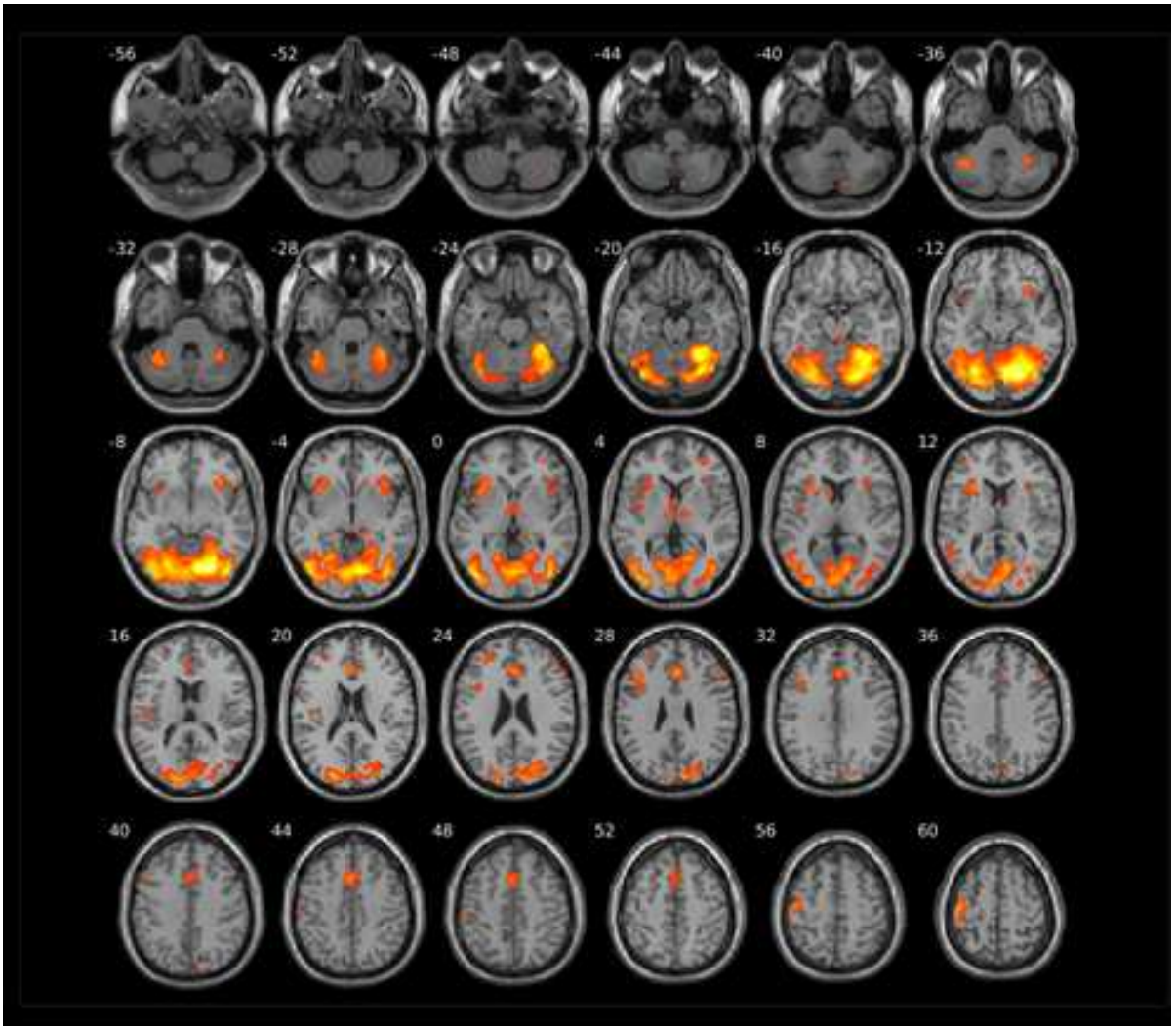

Figure 5.3 illustration of transverse slice brain view from conjunction analysis overlaying Coherent Motion Sensitivity task and Full-Field Sinusoidal Grating task brain activities (generated by xjView 10.0.)

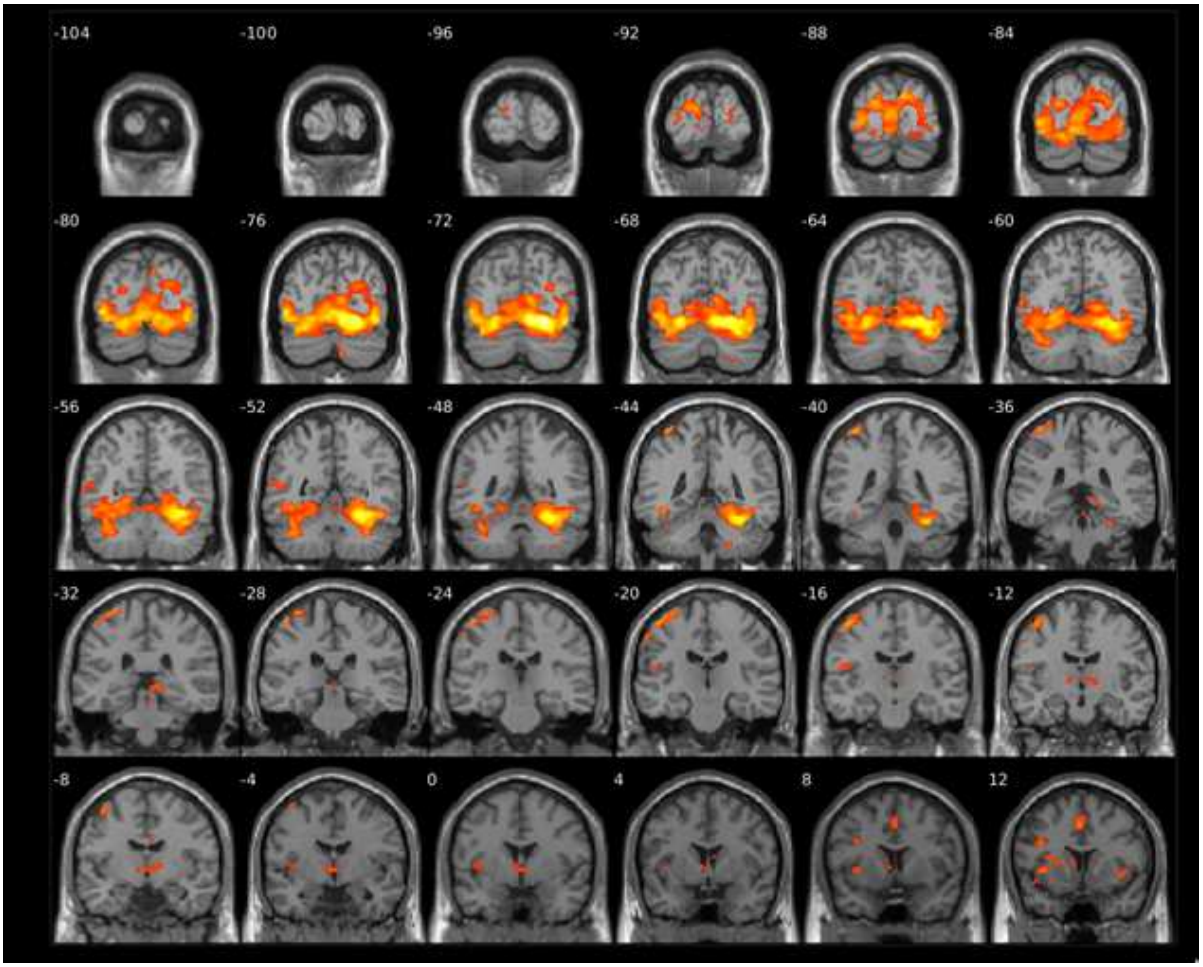

Figure 5.4 illustration of coronal slice brain view from conjunction analysis overlaying Coherent Motion Sensitivity task and Full-Field Sinusoidal Grating task brain activities (generated by xjView 10.0.)

Based on the conjunction analysis as well as previous literature review, the brain regions decided for VOI extraction include: : MFG_R, MFG_L, V5_R, V5_L, CRUS I_R, CRUS I_L, V1_B. VOI selection is illustrated below in the Figure 5.5.

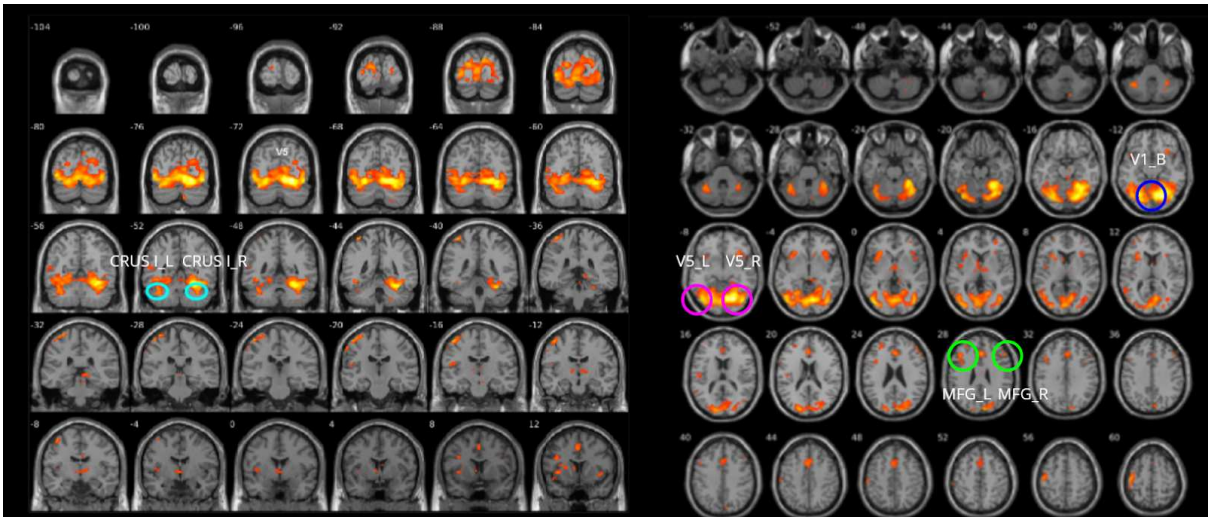

Figure 5.5 illustrates the conjunction analysis brain activity and chosen regions. Green represents Middle Frontal gyrus; purple represents V5; light blue represents Crus I; dark blue represents bilateral V1.

5.2 DCM subject level analysis

Standard pipeline for a subject level analysis, encompassing DCM Specification, DCM Estimation and DCM Diagnosis was performed on all subjects, demonstrated here with a randomly chosen subject. Region locations are shown in Figure 5.6. Results of estimation are represented in Figure 5.7. Additionally, multiple different results can be reviewed at this point including Intrinsic Connectivity (Figure 5.8) and Output (5.9). Finally, diagnostic results are represented in Figure 5.10.

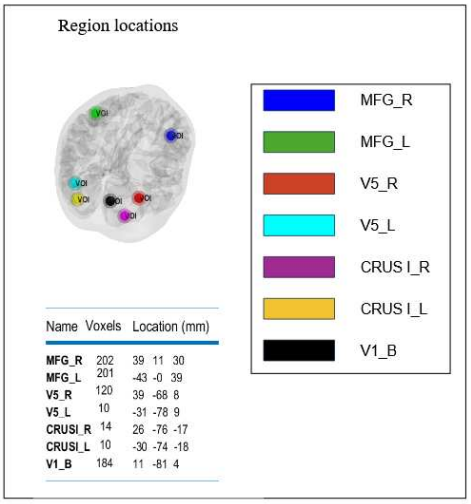

Figure 5.6 illustrates region locations of both groups with green and dark blue representing MFG left and right respectively, light blue and red representing V5 left and right respectively, yellow and purple representing Crus I left and right respectively and black representing bilateral V1. At the bottom is a table representing region name, number of voxels and location of the region.

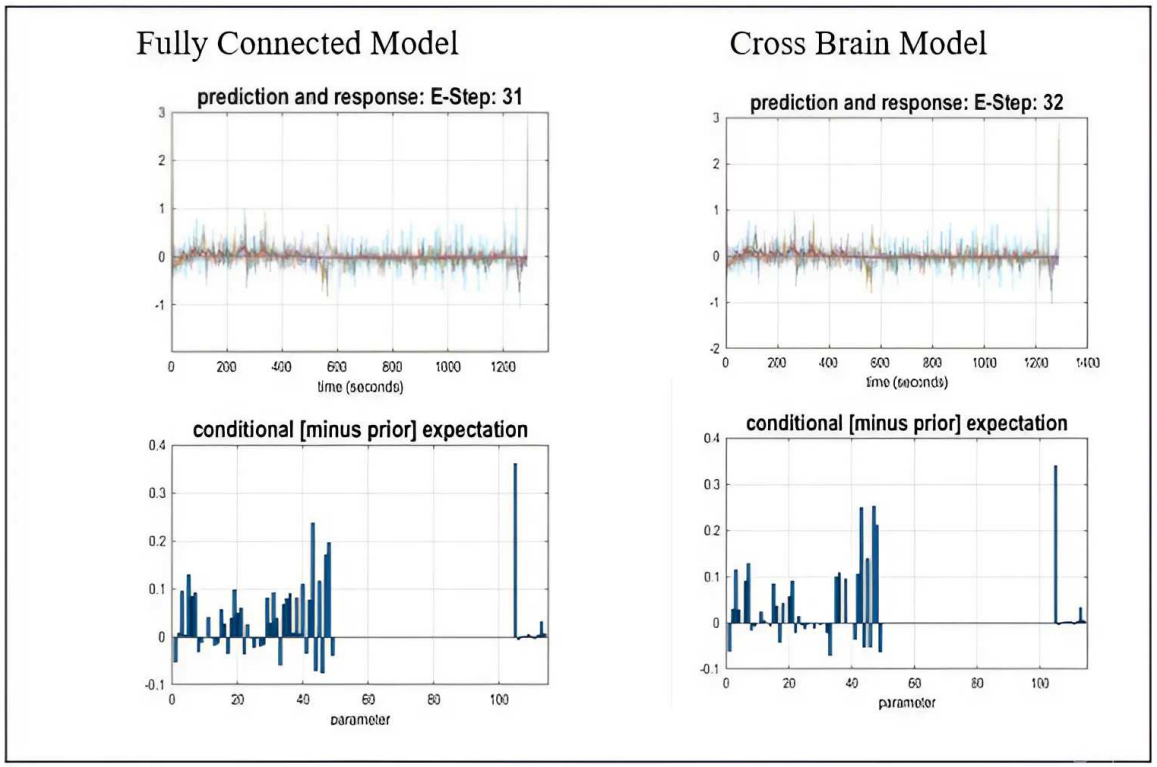

Figure 5.7 Estimation for a random subject Fully Connected Model (left) and Cross Brain Model (right)

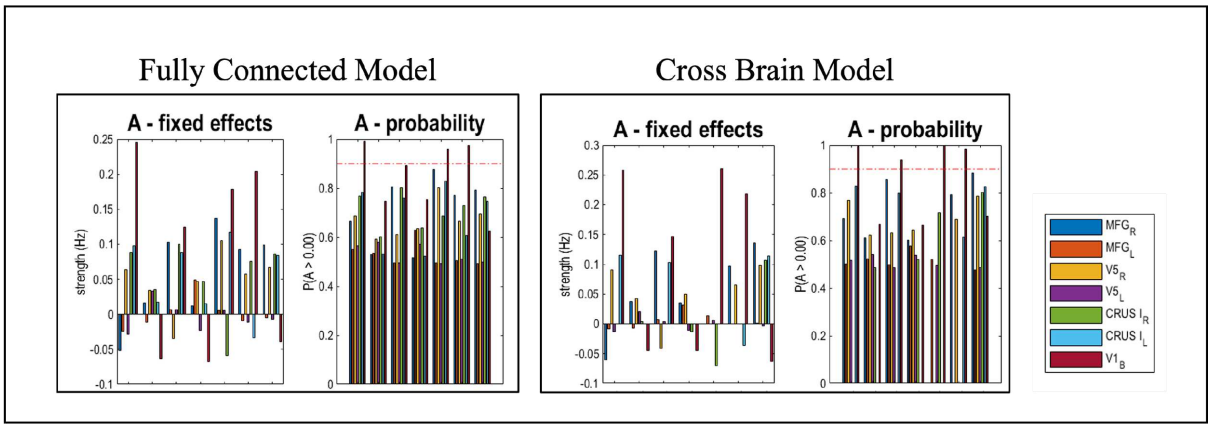

Figure 5.8 illustrates random subject parameter estimates for the endogenous coupling for Fully Connected Model (left) and Cross Brain Model (right)

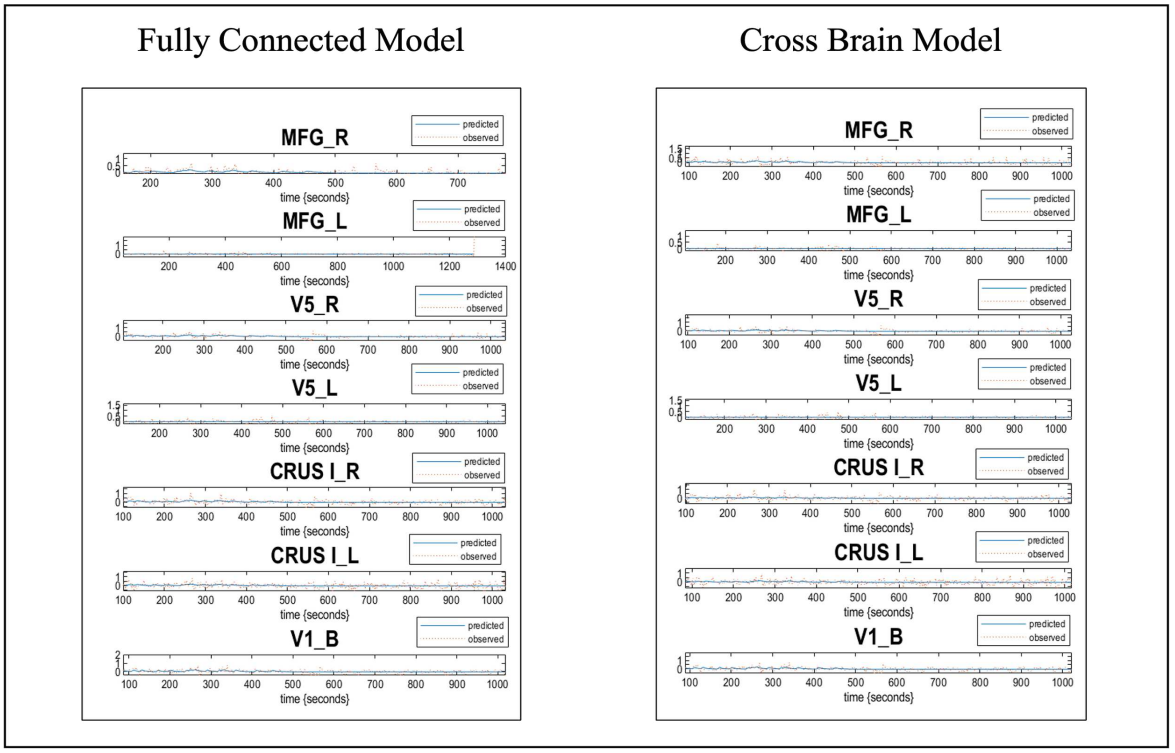

Figure 5.9. illustrates random subject outputs for Fully Connected Model (left) and Cross Brain Model (right). Output signal (Hz) for predicted (blue line) and observed response (red dots) of each ROIs in time (seconds).

Further, DCM Diagnostic was performed in Matlab (MathWorks Inc., 2023) using <spm_dcm_fmri_check(GCM)>, in order to gather more information on the estimated model. Figure 5.10 represents the diagnostic check for TR and DD groups respectively. On both figures present is a model of the selected subject, where bold lines are the predicted timeseries of regions, dotted lines are the data.

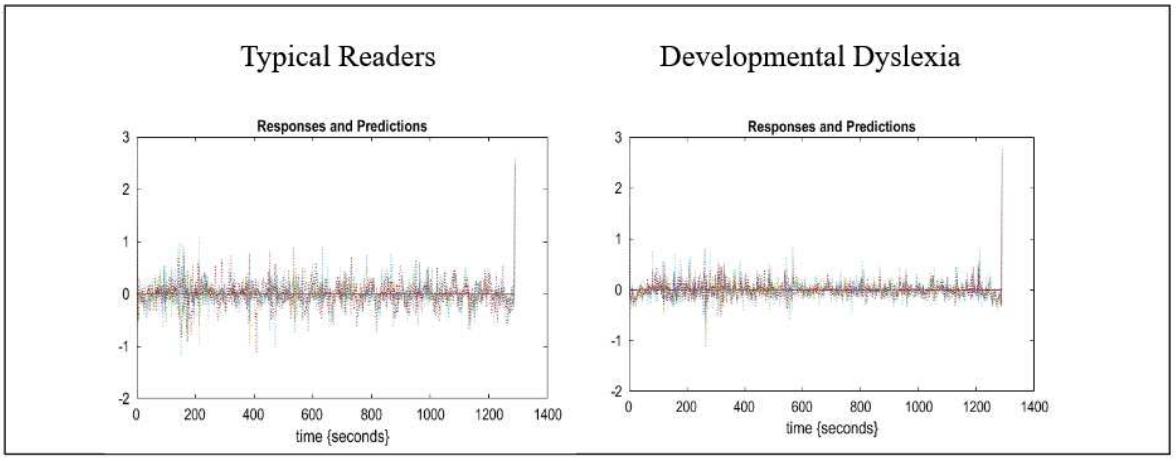

Figure 5.10 Diagnostic for TR group (left) and DD group (right)

5.3 Bayesian Model Averaging

Hypothesis for testing the differences in effective connectivity dynamics between typical readers and developmental dyslexia in both Fully Connected and structurally informed Cross Brain Models created. The BMA results of the typical reader (TR) group and Developmental Dyslexia (DD) group in the Fully Connected model, as well as in the Cross Brain model were compared with the resulting matrices show the connectivity changes between groups, illustrated in the Figure 5.11 and 5.12. Effective connectivity strength represented in Hz with positive (red) values for excitatory connections and negative (blue) values for inhibitory connections. White values correspond to extrinsic connections not included in the model. Self-connectivity (diagonal) cannot be null by definition (see Methods) and it shows a remarkable intrinsic activity of all the regions involved (Figure 5.11 and Figure 5.12). The strongest excitatory connections are from V1_B to MFG_R, CRUS I_R and CRUS I_L in TR for both models. In DD group the strongest excitatory connections for both models are from V5_R to CRUS I_L; from CRUS I_R to V5_L and B1_B; from CRUS I_L to V5_R. Additionally, for DD group only in the Fully Connected model excitatory connection can be seen from CRUS I_R to V5_R and CRUS I_L. Connections that present a different connectivity strength in two groups are highlighted with a *, and with a triangle (Δ) highlighted is the connectivity inversion (from excitatory to inhibitory connectivity change between groups).

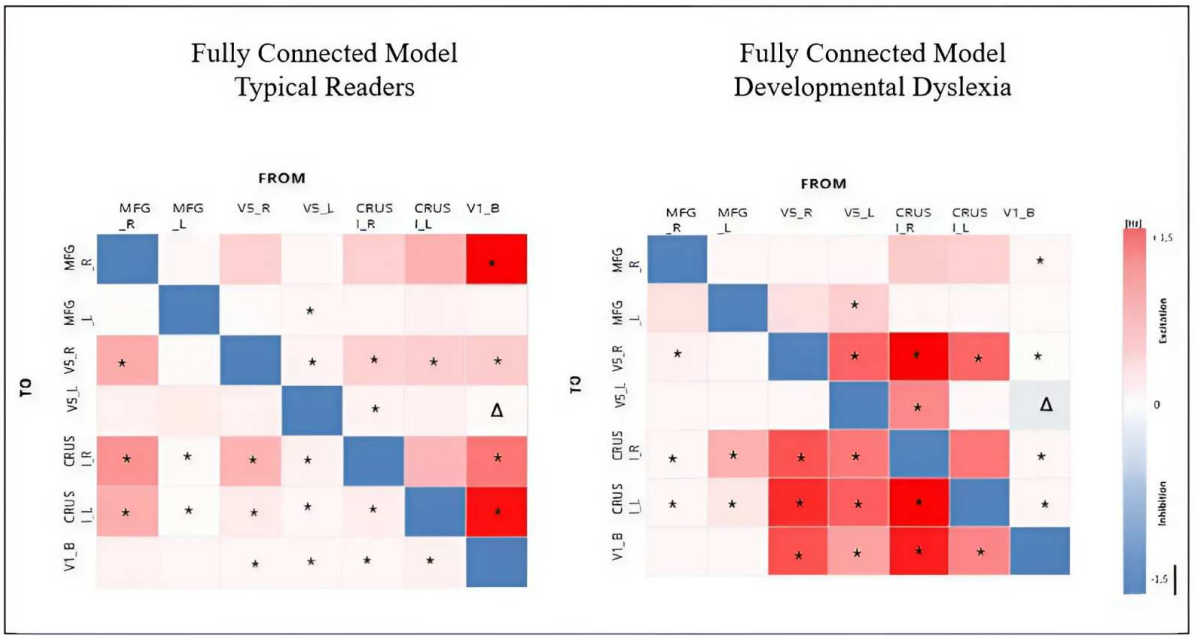

Figure 5.11 illustrates BMA results in typical readers (left) and developmental dyslexia (right) for the Fully Connected Model. Connectivity differences between two groups are represented with a star (*).

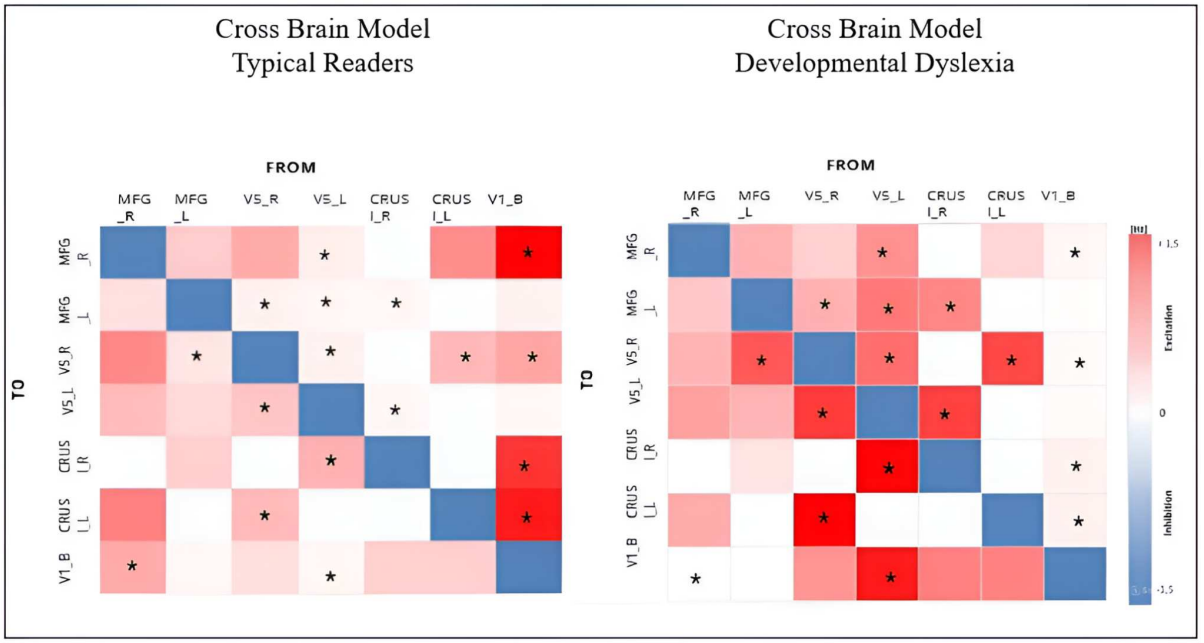

Figure 5.12 illustrates BMA results in typical readers (left) and developmental dyslexia (right) for the Cross Brain Model. Connectivity differences between two groups are represented with a star (*).

6. Discussion

The present study examined effective connectivity in developmental dyslexia (DD) and typical readers (TR) using Dynamic Causal Modeling (DCM) with a focus on seven regions of interest: the left and right middle frontal gyri, left and right middle temporal visual area (V5), left and right Crus I of the cerebellum, and bilateral primary visual cortex (V1). The specific nodes involved are consistent with the literature that highlights the multifaceted nature of developmental dyslexia, encompassing visual, cognitive, and motor components. The left medial frontal gyrus, for example, is part of the Ventral Attention Network, often affected in developmental dyslexia (Vossel et al., 2013). Similarly, V5, part of the magnocellular pathway, is associated with motion detection and visual processing, areas where dyslexic individuals may exhibit deficits (Stein, 2019). The cerebellum's role in motor control and reading, and its involvement in developmental dyslexia based on the Cerebellar Deficit Theory warranted its place among the decided nodes (Stoodley & Stein, 2013).

We proposed a hypothesis that states:

H: there is a difference in effective connectivity between typical readers and developmental dyslexia groups in both Fully Connected and structurally informed Cross Brain Models constructed based on the structural connectivity information for the cerebellum and cerebrum.

The Fully Connected Model takes into account all possible direct connections between brain regions. In contrast, the Cross Brain Model incorporates structural connectivity information into the functional DCM analysis. This approach utilizes anatomical data to inform and constrain the functional connectivity models in DCM, in order to create more biologically plausible and accurate representations of brain connectivity by integrating knowledge of the underlying anatomical pathways. Moreover, our findings support the hypothesis, indicating significant differences in effective connectivity between typical readers and individuals with developmental dyslexia in both Fully Connected and structurally informed Cross Brain Models. The differential connectivity patterns observed may reflect the neurobiological underpinnings of the difficulties typically experienced by individuals with dyslexia.

In the Fully Connected Model, majority of the connectivity changes were hyperactivations in DD group, consistent with a study done by Morken et al. (2014), to and from cerebellar regions right Crus I and left Crus I both ipsi- and contralaterally with cerebral regions,

indicating possible need for increased effort by those with dyslexia. Notably, connectivity inversion (i.e., change from excitatory to inhibitory connection) occurred from bilateral V1 to left V5 between TR and DD possibly explaining the disruptions in visual processing pathways that may contribute to the reading difficulties in DD. On the contrary, in the Cross Brain Model, no inversions were present which suggests stable and predictable directional interactions between the cerebrum and cerebellum based on structural connectivity, while the majority of difference in connectivity was between cerebral regions, once more showing hyperactivity in DD group consistent with the literature (Morken et al. 2014). The cerebro-cerebellar connectivity differences that did occur were mostly from cerebellar regions to the contralateral cerebral regions. These results align with Deco et al. (2021) who delve into the dynamic implications stemming from regional heterogeneity in the brain. Their analysis posits that variations in gene expression profiles across distinct brain regions intricately influence inter-regional interactions and communication pathways, which could underlie the observed patterns of cerebro-cerebellar connectivity in dyslexia. Specifically, perturbations in gene expression within key brain regions associated with developmental dyslexia may disrupt normal cerebro-cerebellar interactions, thereby impacting critical cognitive functions such as reading and language processing. Both models indicated a major connectivity difference in the form of hypoactivity in DD from the main input region bilateral V1 to MFG_R, V5_R, CRUS I_R, CRUS I_L. Hypoactivity in Ventral Visual Stream has been consistently found in dyslexia (Sigurdardottir et al., 2021). Additionally, the Fully Connected Model showed major connectivity changes from all the other regions, excluding MFG_R and MFG_L as well as V1_B itself, to bilateral V1.

Our study contributes to the neuroscientific literature by employing Dynamic Causal Modeling (DCM) to investigate differences in causal, directional interactions and symmetry-breaking dynamics within brain networks between those with dyslexia and typical readers during attention tasks. Unlike traditional assessments of structural and functional connectivity, DCM allows us to discern how specific neural regions causally influence one another over time, thus offering a more nuanced understanding of cognitive functions. Furthermore, Battaglia et al. (2012) highlight the importance of dynamic changes in connectivity rather than static connections, additionally illustrating the complex nature of effective connectivity, where interactions between brain regions evolve dynamically based on task demands and cognitive processes. Integrating these perspectives enhances our understanding of how directional causal interactions and symmetry-breaking dynamics in

brain connectivity contribute to the cognitive differences observed between those with dyslexia and typical readers.

Implications

This study contributes to a broader understanding of how the brain supports complex cognitive functions. The findings emphasize the need for models of brain connectivity that integrate structural and functional data, acknowledging that effective connectivity can often diverge from the direct anatomical pathways due to the dynamic and adaptive nature of neural processing.

These findings have several important implications for understanding developmental dyslexia. Firstly, our findings prove the importance of taking into account both functional and structural connectivity in understanding the neural mechanisms underlying dyslexia. While structural connectivity provides a map of potential connections, functional and effective connectivity analyses reveal how these connections are utilized during specific tasks (Rykhlevskaia et al., 2008). Integrating causality assessments in the context of cerebro-cerebellar interactions not only enhances our comprehension of neural network dynamics but also illuminates potential mechanisms underlying dyslexia at the level of brain circuitry (Bukhari et al., 2022). Therefore, the differences in effective connectivity patterns between typical readers and dyslexic individuals highlight potential targets for interventions. Additionally, understanding these connectivity patterns could help in the early identification of children at risk for dyslexia, as different connectivity patterns might be used as a neuronal marker of DD, allowing for earlier and more targeted intervention strategies.

Future studies could explore alternative modeling approaches or incorporate additional data types in order to refine the understanding of the interaction between structural and functional connectivity. Additionally, longitudinal studies could investigate how connectivity patterns evolve with interventions designed to improve reading and attention skills in individuals with dyslexia, potentially offering insights into the plasticity of the brain. Further research can also expand to include other neurodevelopmental disorders that affect reading, attention and language processing. By comparing connectivity patterns across different conditions, we can begin to identify similarities and differences that might inform more general theories of brain development and function. Lastly, associating the results with clinical scores of TR and DD the original study by Mascheretti and colleagues (2021) has conducted and provided would

allow for improvement in identification and diagnosing of developmental dyslexia, and should therefore be considered as a future direction.

Limitations

While this study provides valuable insights into the effective connectivity differences between typical readers and developmental dyslexia groups, several limitations should be acknowledged.

1. Exclusion of the Full-Field Sinusoidal Grating Task: The decision to exclude the Full-Field Sinusoidal Grating task after the conjunction analysis represents a limitation. This exclusion was primarily due to the insufficiently captured brain activity with the passive nature of the task and therefore its incompatibility with DCM methodology.

2. Decreased Participant Pool: Another limitation stems from the decreased number of participants involved in the study. This reduction was partially due to the exclusion of participants exhibiting minimal brain activity during the tasks. Additionally, the original sample size consisted of 90 participants, however the decision to match the participant demographics with Mascheretti et al. (2021), as well as the correct genetic variant incidence in the general population, led to a further decrease in the sample size. While this approach aims to enhance comparability and facilitate cross-study analyses, it inherently limits the statistical power of our findings and may introduce biases into the results.

3. Generalizability of Findings: The findings of this study may not be fully generalizable to broader populations beyond the specific age range, demographics, and task paradigms employed. The sample primarily consisted of individuals from a specific geographical region, potentially limiting the generalizability of our findings to more diverse populations. Moreover, the task paradigms utilized may not fully capture the complexity of developmental dyslexia in real-world contexts.

4. Cross-sectional Design: The cross-sectional design of this study represents another limitation. While it provides valuable insights into the differences in effective connectivity between typical readers and developmental dyslexia groups at a specific time point, it precludes the assessment of longitudinal changes or causal relationships over time. Future longitudinal studies are needed to explain the developmental trajectories of effective connectivity alterations in developmental dyslexia and the potential impact of interventions on these patterns.

5. DCM Constraints: One significant limitation of using Dynamic Causal Modeling (DCM), as highlighted by Lohmann et al. (2012), is the practical constraint on the maximum number of nodes that can be included in the model. DCM is computationally intensive, and as the number of nodes increases, the model's complexity grows exponentially. This constraint restricts the ability to fully capture the intricacies of large-scale brain networks, potentially resulting in oversimplified models. Additionally, DCM can be highly sensitive to the chosen model structure, and with many possible configurations, determining the most accurate model that truly represents the underlying neural processes can be challenging. This issue can lead to difficulties in validating the findings and ensuring that the inferred connectivity patterns are genuine reflections of brain connectivity rather than artifacts of the model selection process.

Addressing these limitations in future research will be essential to further explain the neural mechanisms underlying developmental dyslexia and advance our ability to develop targeted interventions tailored to individual neurobiological profiles.

6. Conclusion

In summary, this study provides evidence for altered effective connectivity in developmental dyslexia compared to typical readers in the full connectivity dynamics and structurally informed model of the cerebrum and the cerebellum. The findings emphasize the complexity of the neuronal networks involved in attention and the importance of considering both structural and functional aspects of connectivity. These insights contribute to a deeper understanding of the neurobiological basis of developmental dyslexia and highlight the need for further research to integrate these dimensions comprehensively.

The confirmation of our hypothesis provides a solid foundation for future investigations into the neural mechanisms of developmental dyslexia. By continuing to refine our models and incorporate a broader range of data, we can move closer to a comprehensive understanding of how the brain supports cognitive processes and how these processes go awry in developmental dyslexia. This knowledge will be crucial for developing more effective diagnostic tools and interventions, ultimately improving outcomes for individuals with dyslexia.

7. Bibliography

1. Amaro, E., & Barker, G. J. (2006). Study design in fMRI: Basic principles. *Brain and Cognition*, *60*(3), 220–232. https://doi.org/10.1016/j.bandc.2005.11.009

2. American Psychiatric Association. (2006). Diagnostic and statistical manual of mental disorders (4th ed.). American Psychiatric Association.

3. Amunts, K., Mohlberg, H., Bludau, S., & Zilles, K. (2020). Julich-Brain: A 3D probabilistic atlas of the human brain's cytoarchitecture. *Science*, *369*(6506), 988–992. https://doi.org/10.1126/science.abb4588

4. Arina, S., Iervolino, I., & Stella, G. (2013). Prima raccolta di dati normativi per la valutazione della dislessia evolutiva negli adolescenti su un campione di scuola secondaria di secondo grado. Dislessia, 10, 9–38.

5. Ashburner, J., Barnes, G., Chen, C.-C., Daunizeau, J., Flandin, G., Friston, K., Jafarian, A., Kiebel, S., Kilner, J., Litvak, V., Moran, R., Adeel, W., Klaas, R., Sungho, S., Zeidman, T., Gitelman, D., Henson, R., Hutton, C., Glauche, V., & Mattout, J. (2020). *SPM12 Manual The FIL Methods Group (and honorary members)*. https://www.fil.ion.ucl.ac.uk/spm/doc/spm12_manual.pdf

6. Atkinson, J. (1992). Early visual development: Differential functioning of parvocellular and magnocellular pathways. *Eye*, *6*(2), 129–135. https://doi.org/10.1038/eye.1992.28

7. Battaglia, D., Witt, A., Wolf, F., & Geisel, T. (2012). Dynamic effective connectivity of inter-areal brain circuits. PLoS computational biology, 8(3), e1002438.

8. Berger, A., & Posner, M. I. (2000). Pathologies of brain attentional networks. *Neuroscience & Biobehavioral Reviews*, *24*(1), 3–5. https://doi.org/10.1016/s0149-7634(99)00046-9

9. Bertelli, B., & Bilancia, G. (2006). VAUMeLF Batteria per la Valutazione Dell'attenzione Uditiva e Della Memoria di Lavoro Fonologica Nell'età Evolutiva. Organizzazioni Speciali.

10. Boros, M., Anton, J.-L., Pech-Georgel, C., Grainger, J., Szwed, M., & Ziegler, J. C. (2016). Orthographic processing deficits in developmental dyslexia: Beyond the ventral visual stream. *NeuroImage*, *128*, 316–327. https://doi.org/10.1016/j.neuroimage.2016.01.014

11. Briggs, G. G., & Nebes, R. D. (1975). Patterns of Hand Preference in a Student Population. *Cortex*, *11*(3), 230–238. https://doi.org/10.1016/s0010-9452(75)80005-0

12. Brown, R. W., Cheng, Y.-C. . N., Haacke, E. M., Thompson, M. R., & Venkatesan, R. (2014). Magnetic Resonance Imaging: Physical Principles and Sequence Design. In *Google Books*. John Wiley & Sons.

13. Bukhari, Q., Ruf, S. F., Guell, X., Whitfield-Gabrieli, S., & Anteraper, S. (2022). Interaction between cerebellum and cerebral cortex, evidence from dynamic causal modeling. The Cerebellum, 21(2), 225-233.

14. Buxton, R. B., & Frank, L. R. (1997). A Model for the Coupling between Cerebral Blood Flow and Oxygen Metabolism during Neural Stimulation. *Journal of Cerebral Blood Flow & Metabolism*, *17*(1), 64–72. https://doi.org/10.1097/00004647-199701000-00009

15. Chen, J. E., & Glover, G. H. (2015). Functional Magnetic Resonance Imaging Methods. *Neuropsychology Review*, *25*(3), 289–313. https://doi.org/10.1007/s11065-015-9294-9

16. Conners, C. K. (1989). Manual for Conners' Rating Scales. Multi-Health Systems.

17. Conners, C. K., Sitarenios, G., Parker, J. D. A., & Epstein, J. N. (1998). The revised Conners' Parent Rating Scale (CPRS-R): Factor structure, reliability, and criterion validity. Journal of Abnormal Child Psychology, 26, 257–268.

18. Corbetta, M., & Shulman, G. L. (2002). Control of goal-directed and stimulus-driven attention in the brain. *Nature Reviews. Neuroscience*, *3*(3), 201–215. https://doi.org/10.1038/nrn755

19. Cornoldi, C. (1995). Nuove Prove di Lettura MT per la Scuola Media Inferiore. Organizzazioni Speciali.

20. Cornoldi, C., & Colpo, G. (1998). Prove di Lettura MT per la Scuola Elementare (2nd ed.). Organizzazioni Speciali

21. D'Angelo, E. (2018). Physiology of the cerebellum. Handbook of clinical neurology, 154, 85-108.

22. Deco, G., Kringelbach, M. L., Arnatkeviciute, A., Oldham, S., Sabaroedin, K., Rogasch, N. C., & Fornito, A. (2021). Dynamical consequences of regional heterogeneity in the brain's transcriptional landscape. Science Advances, 7(29), eabf4752.

23. Démonet, J.-F., Taylor, M. J., & Chaix, Y. (2004). Developmental dyslexia. *The Lancet*, *363*(9419), 1451–1460. https://doi.org/10.1016/s0140-6736(04)16106-0

24. Desikan, R. S., Ségonne, F., Fischl, B., Quinn, B. T., Dickerson, B. C., Blacker, D., Buckner, R. L., Dale, A. M., Maguire, R. P., Hyman, B. T., Albert, M. S., & Killiany, R. J. (2006). An automated labeling system for subdividing the human cerebral cortex

on MRI scans into gyral based regions of interest. *NeuroImage*, *31*(3), 968–980. https://doi.org/10.1016/j.neuroimage.2006.01.021

25. Diedrichsen, J., Balster, J.H., Cussans, E., Ramnani, N. (2009). A probabilistic MR atlas of the human cerebellum. Neuroimage.

26. Dreizen, P. (2004). The Nobel prize for MRI: a wonderful discovery and a sad controversy. *The Lancet*, *363*(9402), 78. https://doi.org/10.1016/s0140-6736(03)15182-3

27. Eden, G. F., Olulade, O. A., Evans, T. M., Krafnick, A. J., & Alkire, D. R. (2016). Developmental Dyslexia. *Neurobiology of Language*, 815–826. https://doi.org/10.1016/b978-0-12-407794-2.00065-1

28. Fernandez-Duque, D., & Posner, M. I. (2001). Brain Imaging of Attentional Networks in Normal and Pathological States. *Journal of Clinical and Experimental Neuropsychology*, *23*(1), 74–93. https://doi.org/10.1076/jcen.23.1.74.1217

29. Fisher, S. E., & DeFries, J. C. (2002). Developmental dyslexia: genetic dissection of a complex cognitive trait. *Nature Reviews Neuroscience*, *3*(10), 767–780. https://doi.org/10.1038/nrn936

30. Flandin, G., & Penny, W. D. (2007). Bayesian fMRI data analysis with sparse spatial basis function priors. *NeuroImage*, *34*(3), 1108–1125. https://doi.org/10.1016/j.neuroimage.2006.10.005

31. Frazier, J. A., Chiu, S., Breeze, J. L., Makris, N., Lange, N., Kennedy, D. N., Herbert, M. R., Bent, E. K., Koneru, V. K., Dieterich, M. E., Hodge, S. M., Rauch, S. L., Grant, P. E., Cohen, B. M., Seidman, L. J., Caviness, V. S., & Biederman, J. (2005). Structural brain magnetic resonance imaging of limbic and thalamic volumes in pediatric bipolar disorder. *The American Journal of Psychiatry*, *162*(7), 1256–1265. https://doi.org/10.1176/appi.ajp.162.7.1256

32. Friston, K. J., Harrison, L., & Penny, W. (2003). Dynamic causal modelling. *NeuroImage*, *19*(4), 1273–1302. https://doi.org/10.1016/s1053-8119(03)00202-7

33. Friston, K. J., Holmes, A. P., Price, C. J., Büchel, C., & Worsley, K. J. (1999). Multisubject fMRI Studies and Conjunction Analyses. *NeuroImage*, *10*(4), 385–396. https://doi.org/10.1006/nimg.1999.0484

34. Friston, K. J., Preller, K. H., Mathys, C., Cagnan, H., Heinzle, J., Razi, A., & Zeidman, P. (2019). Dynamic causal modelling revisited. *NeuroImage*, *199*, 730–744. https://doi.org/10.1016/j.neuroimage.2017.02.045

35. Galaburda, A. M., LoTurco, J., Ramus, F., Fitch, R. H., & Rosen, G. D. (2006). From genes to behavior in developmental dyslexia. *Nature Neuroscience*, *9*(10), 1213–1217. https://doi.org/10.1038/nn1772

36. Ghadery, C., Pirpamer, L., Hofer, E., Langkammer, C., Petrovic, K., Loitfelder, M., Schwingenschuh, P., Seiler, S., Duering, M., Jouvent, E., Schmidt, H., Fazekas, F., Mangin, J.-F., Chabriat, H., Dichgans, M., Ropele, S., & Schmidt, R. (2015). R2* mapping for brain iron: associations with cognition in normal aging. *Neurobiology of Aging*, *36*(2), 925–932. https://doi.org/10.1016/j.neurobiolaging.2014.09.013

37. Giovannetti, G., Hartwig, V., Positano, V., & Vanello, N. (2014). Radiofrequency Coils for Magnetic Resonance Applications: Theory, Design, and Evaluation. *Critical Reviews in Biomedical Engineering*, *42*(2), 109–135. https://doi.org/10.1615/critrevbiomedeng.2014011482

38. Glover, G. H. (2011). Overview of Functional Magnetic Resonance Imaging. *Neurosurgery Clinics of North America*, *22*(2), 133–139. https://doi.org/10.1016/j.nec.2010.11.001

39. Goldfarb, L., & Shaul, S. (2013). Abnormal attentional internetwork link in dyslexic readers. *Neuropsychology*, *27*(6), 725–729. https://doi.org/10.1037/a0034422

40. Goldstein, J. M., Seidman, L. J., Makris, N., Ahern, T., O'Brien, L. M., Caviness, V. S., Kennedy, D. N., Faraone, S. V., & Tsuang, M. T. (2007). Hypothalamic Abnormalities in Schizophrenia: Sex Effects and Genetic Vulnerability. *Biological Psychiatry*, *61*(8), 935–945. https://doi.org/10.1016/j.biopsych.2006.06.027

41. Gottwald, B., Mihajlovic, Z., Wilde, B., & Mehdorn, H. M. (2003). Does the cerebellum contribute to specific aspects of attention? *Neuropsychologia*, *41*(11), 1452–1460. https://doi.org/10.1016/s0028-3932(03)00090-3

42. Haacke, E. M. (1999). Magnetic resonance imaging: Physical principles and sequence design. In *catalog.loc.gov Library Catalog*. Wiley. https://lccn.loc.gov/99022880

43. Hashemi, R. H., Bradley, W. G., & Lisanti, C. J. (2012). *MRI: The Basics*. Lippincott Williams & Wilkins.

44. Horwitz, B. (2003). The elusive concept of brain connectivity. *NeuroImage*, *19*(2), 466–470. https://doi.org/10.1016/s1053-8119(03)00112-5

45. Huettel, S. A., Song, A. W., & McCarthy, G. (2008). Functional magnetic resonance imaging. In *catalog.loc.gov Library Catalog* (2nd ed). Sinauer Associates. https://lccn.loc.gov/2008054124

46. Huettel, S. A., Song, A. W., & McCarthy, G. (2014). Functional magnetic resonance imaging Third ed. *Sunderland*.

47. Humphreys, G. W., & Sui, J. (2015). Attentional control and the self: The Self-Attention Network (SAN). *Cognitive Neuroscience*, *7*(1-4), 5–17. https://doi.org/10.1080/17588928.2015.1044427

48. Ioannis Tsougos. (2017). *Advanced MR Neuroimaging*. CRC Press.

49. Jobson, K. R., Hoffman, L. J., Metoki, A., Popal, H., Dick, A. S., Reilly, J., & Olson, I. R. (2022). Language and the Cerebellum: Structural Connectivity to the Eloquent Brain. *Neurobiology of Language*, 1–24. https://doi.org/10.1162/nol_a_00085

50. Kahan, J., & Foltynie, T. (2013). Understanding DCM: Ten simple rules for the clinician. *NeuroImage*, *83*, 542–549. https://doi.org/10.1016/j.neuroimage.2013.07.008

51. Karavasilis, E., Christidi, F., Velonakis, G., Giavri, Z., Kelekis, N. L., Efstathopoulos, E. P., Evdokimidis, I., & Dellatolas, G. (2019). Ipsilateral and contralateral cerebro-cerebellar white matter connections: A diffusion tensor imaging study in healthy adults. *Journal of Neuroradiology*, *46*(1), 52–60. https://doi.org/10.1016/j.neurad.2018.07.004

52. Kellermann, T., Regenbogen, C., De Vos, M., Mößnang, C., Finkelmeyer, A., & Habel, U. (2012). Effective Connectivity of the Human Cerebellum during Visual Attention. *The Journal of Neuroscience*, *32*(33), 11453–11460. https://doi.org/10.1523/jneurosci.0678-12.2012

53. Kershner, J. R. (2021). Multisensory deficits in dyslexia may result from a locus coeruleus attentional network dysfunction. *Neuropsychologia*, *161*, 108023. https://doi.org/10.1016/j.neuropsychologia.2021.108023

54. Lewandowska, M., Rafal, M., Malgorzata, G., Elzbieta, W., & Henryk, S. (2014). Attention Dysfunction Subtypes of Developmental Dyslexia. *Medical Science Monitor*, *20*, 2256–2268. https://doi.org/10.12659/msm.890969

55. Lohmann, G., Erfurth, K., Müller, K., & Turner, R. (2012). Critical comments on dynamic causal modelling. Neuroimage, 59(3), 2322-2329.

56. Makris, N., Goldstein, J. M., Kennedy, D., Hodge, S. M., Caviness, V. S., Faraone, S. V., Tsuang, M. T., & Seidman, L. J. (2006). Decreased volume of left and total anterior insular lobule in schizophrenia. *Schizophrenia Research*, *83*(2-3), 155–171. https://doi.org/10.1016/j.schres.2005.11.020

57. Mannarelli, D., Pauletti, C., Currà, A., Marinelli, L., Corrado, A., Delle Chiaie, R., & Fattapposta, F. (2019). The Cerebellum Modulates Attention Network Functioning: Evidence from a Cerebellar Transcranial Direct Current Stimulation and Attention Network Test Study. *The Cerebellum*, *18*(3), 457–468. https://doi.org/10.1007/s12311-019-01014-8

58. Marreiros, A., Stephan, K., & Friston, K. (2010). Dynamic causal modeling. *Scholarpedia*, *5*(7), 9568. https://doi.org/10.4249/scholarpedia.9568

59. Mascheretti, S., Peruzzo, D., Andreola, C., Villa, M., Ciceri, T., Trezzi, V., Marino, C., & Arrigoni, F. (2021). Selecting the Most Relevant Brain Regions to Classify Children with Developmental Dyslexia and Typical Readers by Using Complex Magnocellular Stimuli and Multiple Kernel Learning. *Brain Sciences*, *11*(6), 722. https://doi.org/10.3390/brainsci11060722

60. Mcrobbie, D. W. (2005). *MRI from picture to proton*. Cambridge University Press.

61. Monti, M. M. (2011). Statistical analysis of fMRI time-series: a critical review of the GLM approach. *Front. Hum. Neurosci*, *5*(28). https://doi.org/10.3389/fnhum.2011.00028

62. Morken, F., Helland, T., Hugdahl, K., & Specht, K. (2014). Children with dyslexia show cortical hyperactivation in response to increasing literacy processing demands. *Frontiers in Psychology*, *5*. https://doi.org/10.3389/fpsyg.2014.01491

63. Nicolson, R. I., Fawcett, A. J., & Dean, P. (2001). Developmental dyslexia: the cerebellar deficit hypothesis. *Trends in Neurosciences*, *24*(9), 508–511. https://doi.org/10.1016/s0166-2236(00)01896-8

64. Nobile, M., Alberti, B., & Zuddas, A. (2007). CRS-R. Conners' Rating Scale—Revised. Organizzazioni Speciali.

65. Palesi, F., Tournier, J.-D., Calamante, F., Muhlert, N., Castellazzi, G., Chard, D. T., D'Angelo, E., & Gandini, C. (2015). Contralateral cerebello-thalamo-cortical pathways with prominent involvement of associative areas in humans in vivo. *Brain Structure & Function*, *220*(6), 3369–3384. https://doi.org/10.1007/s00429-014-0861-2

66. Penny, W. D., Stephan, K. E., Daunizeau, J., Rosa, M. J., Friston, K. J., Schofield, T. M., & Leff, A. P. (2010). Comparing Families of Dynamic Causal Models. *PLoS Computational Biology*, *6*(3), e1000709. https://doi.org/10.1371/journal.pcbi.1000709

67. Peters, J. L., De Losa, L., Bavin, E. L., & Crewther, S. G. (2019). Efficacy of dynamic visuo-attentional interventions for reading in dyslexic and neurotypical children: A systematic review. *Neuroscience & Biobehavioral Reviews*, *100*, 58–76. https://doi.org/10.1016/j.neubiorev.2019.02.015

68. Peterson, R. L., & Pennington, B. F. (2012). Developmental dyslexia. *The Lancet*, *379*(9830), 1997–2007. https://doi.org/10.1016/s0140-6736(12)60198-6

69. Peterson, R. L., & Pennington, B. F. (2015). Developmental Dyslexia. *Annual Review of Clinical Psychology*, *11*(1), 283–307. https://doi.org/10.1146/annurev-clinpsy-032814-112842

70. Pieterman, K., Batalle, D., Dudink, J., Tournier, J-Donald., Hughes, E. J., Barnett, M., Benders, M. J., Edwards, A. D., Hoebeek, F. E., & Counsell, S. J. (2016). Cerebello-cerebral connectivity in the developing brain. *Brain Structure & Function*, *222*(4), 1625–1634. https://doi.org/10.1007/s00429-016-1296-8

71. Plewes, D. B., & Kucharczyk, W. (2012). Physics of MRI: A primer. *Journal of Magnetic Resonance Imaging*, *35*(5), 1038–1054. https://doi.org/10.1002/jmri.23642

72. Price, C. J., & Friston, K. J. (1997). Cognitive Conjunction: A New Approach to Brain Activation Experiments. *NeuroImage*, *5*(4), 261–270. https://doi.org/10.1006/nimg.1997.0269

73. Rangaprakash, D., Tadayonnejad, R., Deshpande, G., O'Neill, J., & Feusner, J. D. (2020). FMRI hemodynamic response function (HRF) as a novel marker of brain function: applications for understanding obsessive-compulsive disorder pathology and treatment response. *Brain Imaging and Behavior*, *15*(3). https://doi.org/10.1007/s11682-020-00358-8

74. Raz, A. (2004). Anatomy of attentional networks. *The Anatomical Record*, *281B*(1), 21–36. https://doi.org/10.1002/ar.b.20035

75. Raz, A., & Buhle, J. (2006). Typologies of attentional networks. *Nature Reviews Neuroscience*, *7*(5), 367–379. https://doi.org/10.1038/nrn1903

76. Reynolds, C. R., & Bigler, E. D. (1994). Test of Memory and Learning. Erickson.

77. Rudert, T., & Lohmann, G. (2008). Conjunction analysis and propositional logic in fMRI data analysis using Bayesian statistics. *Journal of Magnetic Resonance Imaging*, *28*(6), 1533–1539. https://doi.org/10.1002/jmri.21518

78. Rykhlevskaia, E., Gratton, G., & Fabiani, M. (2008). Combining structural and functional neuroimaging data for studying brain connectivity: A review. *Psychophysiology*, *45*(2), 173–187. https://doi.org/10.1111/j.1469-8986.2007.00621.x

79. Sartori, G., Job, R., & Tressoldi, P. E. (1995). Batteria per la Valutazione Della Dislessia e Della Disortografia Evolutive. Organizzazioni Speciali.

80. Scerri, T. S., & Schulte-Körne, G. (2009). Genetics of developmental dyslexia. *European Child & Adolescent Psychiatry*, *19*(3), 179–197. https://doi.org/10.1007/s00787-009-0081-0

81. Scerri, T.S., Schulte-Körne, G. Genetics of developmental dyslexia. Eur Child Adolesc Psychiatry 19, 179–197 (2010). https://doi.org/10.1007/s00787-009-0081-0

82. Scott, R. B., Stoodley, C. J., Anslow, P., Paul, C., Stein, J. F., Sugden, E. M., & Mitchell, C. D. (2001). Lateralized cognitive deficits in children following cerebellar lesions. *Developmental Medicine and Child Neurology*, *43*(10), 685. https://doi.org/10.1017/s0012162201001232

83. Sigurdardottir, H. M., Ólafsdóttir, I. M., & Devillez, H. (2021). Words as Visual Objects: Neural and Behavioral Evidence for High-Level Visual Impairments in Dyslexia. *Brain Sciences*, *11*(11), 1427. https://doi.org/10.3390/brainsci11111427

84. Smith-Spark, J. H., & Gordon, R. (2022). Automaticity and Executive Abilities in Developmental Dyslexia: A Theoretical Review. *Brain Sciences*, *12*(4), 446. https://doi.org/10.3390/brainsci12040446

85. Snyder, A. D., Ma, L., Steinberg, J. L., Woisard, K., & Moeller, F. G. (2021). Dynamic Causal Modeling Self-Connectivity Findings in the Functional Magnetic Resonance Imaging Neuropsychiatric Literature. *Frontiers in Neuroscience*, *15*, 636273. https://doi.org/10.3389/fnins.2021.636273

86. Sporns, O. (2007). Brain connectivity. *Scholarpedia*, *2*(10), 4695. https://doi.org/10.4249/scholarpedia.4695

87. Stanovich, K. E. (1988). Explaining the Differences Between the Dyslexic and the Garden-Variety Poor Reader. *Journal of Learning Disabilities*, *21*(10), 590–604. https://doi.org/10.1177/002221948802101003

88. Stein, J. (2001). The magnocellular theory of developmental dyslexia. *Dyslexia*, *7*(1), 12–36. https://doi.org/10.1002/dys.186

89. Stein, J. (2018). What is Developmental Dyslexia? *Brain Sciences*, *8*(2), 26. https://doi.org/10.3390/brainsci8020026

90. Stein, J. (2019). The current status of the magnocellular theory of developmental dyslexia. *Neuropsychologia*, *130*(130), 66–77. https://doi.org/10.1016/j.neuropsychologia.2018.03.022

91. Stein, J. (2023). Theories about Developmental Dyslexia. *Brain Sciences*, *13*(2), 208. https://doi.org/10.3390/brainsci13020208

92. Stephan, K. E., & Friston, K. J. (2010). Analyzing effective connectivity with functional magnetic resonance imaging. *Wiley Interdisciplinary Reviews: Cognitive Science*, *1*(3), 446–459. https://doi.org/10.1002/wcs.58

93. Stephan, K. E., Kasper, L., Harrison, L. M., Daunizeau, J., den Ouden, H. E. M., Breakspear, M., & Friston, K. J. (2008). Nonlinear dynamic causal models for fMRI. *NeuroImage*, *42*(2), 649–662. https://doi.org/10.1016/j.neuroimage.2008.04.262

94. Stephan, K. E., Penny, W. D., Moran, R. J., den Ouden, H. E. M., Daunizeau, J., & Friston, K. J. (2010). Ten simple rules for dynamic causal modeling. *NeuroImage*, *49*(4), 3099–3109. https://doi.org/10.1016/j.neuroimage.2009.11.015

95. Stoet, G., Markey, H., & López, B. (2007). Dyslexia and attentional shifting. *Neuroscience Letters*, *427*(1), 61–65. https://doi.org/10.1016/j.neulet.2007.09.014

96. Stoodley, C. J. (2014). Distinct regions of the cerebellum show gray matter decreases in autism, ADHD, and developmental dyslexia. *Frontiers in Systems Neuroscience*, *8*(92). https://doi.org/10.3389/fnsys.2014.00092

97. Stoodley, C. J., & Stein, J. F. (2012). Cerebellar Function in Developmental Dyslexia. *The Cerebellum*, *12*(2), 267–276. https://doi.org/10.1007/s12311-012-0407-1

98. Taran, N., Farah, R., DiFrancesco, M., Altaye, M., Vannest, J., Holland, S., Rosch, K., Schlaggar, B. L., & Horowitz-Kraus, T. (2022). The role of visual attention in dyslexia: Behavioral and neurobiological evidence. *Human Brain Mapping*, *43*. https://doi.org/10.1002/hbm.25753

99. The MathWorks Inc. (2023). (R2023a), Natick, Massachusetts: The MathWorks Inc. https://www.mathworks.com

100. Thiebaut de Schotten, M., Dell'Acqua, F., Forkel, S., Simmons, A., Vergani, F., Murphy, D. G. M., & Catani, M. (2011). A Lateralized Brain Network for Visuo-Spatial Attention. *Nature Precedings*. https://doi.org/10.1038/npre.2011.5549.1

101. Valdois, S. (2022). The visual‐attention span deficit in developmental dyslexia: Review of evidence for a visual‐attention‐based deficit. *Dyslexia*, *28*(4). https://doi.org/10.1002/dys.1724

102. Voss, M. W. (2016). The Chronic Exercise–Cognition Interaction. *Elsevier EBooks*, 187–209. https://doi.org/10.1016/b978-0-12-800778-5.00009-8

103. Wechsler, D. (2006). Wechsler Intelligence Scale for Children (3rd ed.). Organizzazioni Speciali.

104. Weishaupt, D., Köchli, V. D., & Marincek, B. (2006). *How does MRI work? An introduction to the physics and function of magnetic resonance imaging* (2nd ed.). Springer Berlin Heidelberg. https://doi.org/10.1007/978-3-540-37845-7

105. Williams, J., & O'Donovan, M. C. (2006). The genetics of developmental dyslexia. *European Journal of Human Genetics*, *14*(6), 681–689. https://doi.org/10.1038/sj.ejhg.5201575

106. Zeidman, P., Jafarian, A., Corbin, N., Seghier, M. L., Razi, A., Price, C. J., & Friston, K. J. (2019a). A guide to group effective connectivity analysis, part 1: First level analysis with DCM for fMRI. *NeuroImage*, *200*, 174–190. https://doi.org/10.1016/j.neuroimage.2019.06.031

107. Zeidman, P., Jafarian, A., Corbin, N., Seghier, M. L., Razi, A., Price, C. J., & Friston, K. J. (2019b). A guide to group effective connectivity analysis, part 2: Second level analysis with PEB. *NeuroImage*, *200*, 12–25. https://doi.org/10.1016/j.neuroimage.2019.06.032.

108. Zhang, Y., Wang, Z., Cai, Z., Lin, Q., & Hu, Z. (2016). Nonlinear estimation of BOLD signals with the aid of cerebral blood volume imaging. *BioMedical Engineering OnLine*, *15*(1). https://doi.org/10.1186/s12938-016-0137-6

Acknowledgements

Appendix

	Typical Readers					Developmental Dyslexia				
	Min	Max	Mean (SD)	Skewness	Kurtosis	Min	Max	Mean (SD)	Skewness	Kurtosis
IQ total	80	159	128.25	-0.95	1.37	80	131	104.05	0.11	-0.99
TR accuracy	-0.13	1.42	0.62	0.06	0.85	-12.01	5.19	-3.98	-0.4	0.73
TR speed	-1.00	1.18.	0.18	0.05	-0-63	-4.21	-0.09	-2.62	0.60	0.14
SWR accuracy	-0.67	1.00	0.32	-0.13	-1.16	-10.00	0.33	-3.19	-0.98	0.68
SWR speed	-1.11	0.83	0.01	-0.28	-0.88	-10.12	-0.14	-3.79	-1.48	2.49
SPWR accuracy	-0.67	1.33	0.44	-0.24	0.12	-8.50	0.33	-2.54	-1.48	3.63
SPWR. speed	-1.03	1.15	0.20	-0.25	-0.89	-9.42	-0.67	-3.40	-1.38	1.08
SLFS	-1.35	1.35	0.16	-0.76	0.14	-2.30	0.65	-1-77	0.57	0.72
SLBS	-1.35	1.60	-0.06	0.67	-0.68	-2.2	1.35	-0.72	1.00	2.26
SDFS	-2.00	1.00	0.57	0.07	-0.27	-2.20	0.00	-1.38	0.49	0.22
SDBS	-1.40	2.00	0.57	0.98	-0.06	-1.35	0.65	-0.57	0.62	0.97
SNWR	-2.79	3.00	1.18	-1.40	1.85	-7.00	3.53	-1.63	-0.13	-0.53

Table 2 illustrates the participants' clinical scores conducted and provided by Mascheretti et al. 2021. Tr - text reading; Swr- single word reading; Spwr- single pseudo word; Slfs- single letter forward pan; Slbs - backwards; Sdfs - single digit forward; Sdbs - backward; Snwr - single non word repetition